Characterisation of phosphate mineralogy in Montebras-en-Soumans Pegmatite, Massif Central, France

Cassian Pirard[1,2,3]

1. Laboratoire de Minéralogie et de Cristallochimie, Département de Géologie, Université de Liege, Liege, Belgium

2. Research School of Earth Sciences, College of Science, Australian National University, Canberra, Australia

3. EGRU, Earth & Environmental Sciences, College of Science and Engineering, James Cook University, Townsville, Australia.

**corresponding author: cassian.pf.pirard@gmail.com*

Foreword

This document is a draft that might be published in the future with additional co-authors. Considering the interest regarding a poster presented at an International Symposium in Porto in 2007, it seems appropriate to provide a full dataset in English on this subject. This draft is not peer-reviewed so data and interpretation should be exploited carefully.

Abstract

Montebras-en-Soumans pegmatitic cupola hosts large pods of phosphate composed of primary amblygonite-montebrasite. These aluminium phosphate masses are considerably altered by post-magmatic processes producing a number of secondary metasomatic hydrothermal phosphates (lacroixite, wardite, morinite, viitaniemiite, apatite, triplite, eosphorite) and low-temperature phosphates (apatite, crandallite, goyazite, gorceixite, variscite, turquoise, wavellite). Also found in this study are a Mn-rich viitaniemiite-like phase and an unknown Na-Al-P fluoride. A number of techniques are used to characterise these mineral phases including optical studies, cathodoluminescence (cold & hot), electron-probe micro-analysis (wavelength & energy dispersive spectra), X-ray diffraction, laser ablation inductively coupled plasma mass spectroscopy and infrared spectroscopy.

Keywords: Pegmatite, aluminium phosphates, amblygonite-montebrasite, Montebras, cathodoluminescence, trace elements

Résumé

Le coupole pegmatitique de Montebras-en-Soumans contient de larges masses de phosphates composés essentiellement d’amblygonite-montebrasite primaire. Ces accumulations de phosphates d’aluminium sont considérablement altérées par des processus post-magmatiques, produisant de nombreux phosphates métasomatiques et hydrothermaux secondaires (lacroixite, wardite, morinite, viitaniemiite, apatite, triplite, eosphorite) et des phosphates de basse température (apatite, crandallite, goyazite, gorceixite, variscite, turquoise, wavellite). Cette localité minéralogique contient également une phase manganèsifere similaire à la viitaniemiite et un fluorure de Na-Al-P de nature indéterminée. Des techniques variées sont utilisées pour caractériser ces phases minérales

dont des études optiques, cathodoluminescence (froide et chaude), micro-analyse électronique (longueur d'onde et énergie), diffraction de rayons X, spectroscopie de masse a plasma a couplage inductif à ablation laser et spectroscopie infrarouge.

Mots-clés: Pegmatite, phosphates d'aluminium, amblygonite-montebrasite, Montebras, cathodoluminescence, éléments en traces

1. Introduction

Phosphate minerals in granitic pegmatites environments are a minor but common group of minerals in these magmatic settings. Their sensitivity to changes in geochemical conditions that occur upon cooling and later alteration leads to the formation of a large number of secondary phosphate phases (Mason, 1941; Moore, 1982; Fransolet, 2007).

Here, we provide a mineralogical description and characterisation of the phosphate assemblage in the pegmatite body of Montebras-en-Soumans, Massif Central, France. Alfred Lacroix described the mineralogy of this ore body more than a century ago (Lacroix, 1910), leading to the discovery, among many other minerals of new phosphate species morinite (Lacroix, 1891) and montebrasite (Moissenet, 1871). Although some studies have been done (Aubert, 1969; Marcoux et al., 2021), new mineralogical data was scarcely collected on this mineral deposit and reassessment of the phosphate assemblage, its chemical composition, properties and implications for the pegmatite parageneses is due.

2. Geological background

The Montebras pegmatite is a famous locality-type deposit in the Massif Central, France [N46º19’16’’, E2º17’46’’]. It lies on the northwest margin of the Hercynian belt and is a complex of an albite leucogranite and microgranite intruded in the peraluminous Chanon granitic batholith.

The Montebras albite leucogranite (~310±5 Ma; Melleton et al., 2015; Marcoux et al., 2021), emplaced between and corroding microgranite and Chanon batholith, forms in its uppermost part a metre-thick cupola of albite-muscovite with a pegmatite body, a quartz-rich layer and a mica-rich greisen (Aubert, 1969; Dudoignon et al., 1988; Charoy & Noronha, 1999).

The pegmatite facies (stockscheider) is mostly K-feldspar with some quartz, albite, Li-bearing micas, apatite, topaz and some centimetre-sized amblygonite-montebrasite, some turquoise pods and kaolinite and some cassiterite, W, Cu and As mineralization. It transitions into a quartz-rich layer (quartzglöcke) through decreasing modal feldspars content and contain large aggregates of cassiterite, muscovite, blue apatite and large blocks of Al-rich phosphates (Moissenet, 1871; Aubert, 1969; Marcoux et al., 2021).

The albite-muscovite body has been successively mined possibly for variscite and/or turquoise in prehistoric times (Balagny, 1939), for tin by Celts and possibly Romans (Daubrée, 1868; de Cessac & Chaussat, 1886) and in the 19th century (Mallard, 1859) and for amblygonite and feldspar in the first part of the 20th century (Aubert, 1969). Recently, new mining activities for feldspar have led to a recharacterization of the orebody (Marcoux et al., 2021).

Samples used in this study mostly come from the quartz-rich facies and are part of collections at the University of Liege (ULiege) and the School of Mines of Paris. It contains several samples collected by Alfred Lacroix in the original mineralogical study of this deposit (Lacroix, 1891, 1910) (Table 1).

Table 1. List of samples

MONTEBRAS-EN-SOUMANS (France)				
MONT1	179			
MONT1	43			
MONT2	A607			
MONT3	Montebras		collected by Bourguignon	
MONT4		28889	Bernard, 27-M1766	27-M1766
MONT5		38507	collected by Mallard, 1885	
MONT6		32465	Mine Le Communal	
MONT7		17352	SCEM, 1965	
MONT8		39950		
MONT9		4837	collected by Lacroix, 1890	3-M5847
MONT10		28732	Bertrand Emile collection	1871 (Adam 4485)
MONT11		52512		
MONT12		5838	collected by Morineau, 1891	M6192
MONT13		51297		
MONT14		7836		19.5241
MONT15	Montebras			

3. Analytical techniques

Samples were extensively studied with a binocular lens and optical microscope Leica DMLP at the Laboratory of Mineralogy and Crystallography (ULiege). However, issues arising in the standard microscopical study of aluminium phosphates led us to perform many microscopic observations with cathodoluminescence (See 3.1.).

Identification of less common mineral species was done using X-ray diffraction (XRD) on a Philips PW-3710 diffractometer with a graphite monochromator and a CuKα (λ = 1.5418 Å) or FeKα (λ = 1.9373 Å) radiation source at the Laboratory of Mineralogy and Crystallography (ULiege). For microscopic grains, XRD was done on a Debye-Scherrer camera (diameter = 114.6 mm) mounted on the same X-ray sources. Unit-cell parameters were calculated through least-square refinement program LCLSQ v.8.4 (Burnham, 1991), using *d* values corrected on an internal $Pb(NO_3)_2$ standard.

Chemical analyses were mostly done using electron microprobe CAMECA SX-50 (Ruhr-Universität Bochum) with 15 kV and 8 nA conditions with a 10 μm beam diameter. Standard were jadeite (Na), synthetic glasses (K, Ba), spessartine (Al, Mn), andradite (Si, Fe, Ca), graftonite (P), $SrCu_4Si_4O_{10}$ (Sr, Cu), pyrope (Mg) and topaz (F). The counting time per element is 30 s and 15 s for the most beam-sensitive phases. Fluorine has a 120 s counting time on a PC0 crystal. Beam-sensitive phases analyses were doubled checked with a JEOL 6400 SEM at the Electron Microscopy Unit of the Australian National University (ANU) using Energy Dispersive Spectra (EDS) calibrated on known mineral standards, operating at 15 kV, 1 nA with a 1 μm beam diameter with 120 s counting time. Fluorine in lacroixite, apatite, morinite and phase F have been analysed on JEOL JXA8200 at the Advanced Analytical Centre (JCU) using a 15 kV acceleration voltage, 14.5 nA current. Fluorine is measured using a time-zero integrated analysis where FKα is monitored for 35 s on TAP crystal and regressed to provide an initial value.

Infrared spectra were obtained on a Nicolet Nexus at the Laboratory of Mineralogy and Crystallography (ULiege) between 400 and 4000 cm^{-1} through 32 scans with a 1 cm^{-1} resolution. Infrared source is heated SiC (Ever-Glo). Samples were prepared through a mixture with KBr (1:74) producing a 150 mg pressed pellet dried at 110ºC and analysed in a dry atmosphere.

3.1. Cathodoluminescence applied to aluminium phosphates

Most aluminium phosphates are colourless mineral phases with similar relief (Fig. $1a_1$ & $1b_1$) and low birefringence (Fig. $1a_2$ & $1b_2$) making valuable observations and mineralogical, petrological and textural interpretations based on thin section very difficult. The lack of efficient discrimination between aluminium phosphates in standard optical microscopy was circumvented by performing many microscopic observations with cathodoluminescence (CL) as mineral phases and generations react differently under an electrical current. Paragenesis and textural determination

were mostly done using an Olympus BX50 microscope and a CITL cold cathode luminescence 8200 mk3 housed by the EDDyLab (ULiege). Observations were made at 0.05 mbar with an electronic current of 15±2 kV and 700±50 μA. Cathodoluminescence spectra were obtained with a hot cathode system on a JEOL JXA8200 at the Advanced Analytical Centre (JCU) and processed with XCLent software.

As seen in section 4, cathodoluminescence is a very appropriate tool to apply to these colourless minerals as they have varied responses and their mineral assemblages are mostly free of luminescence quenchers. In the host primary phase (amblygonite-montebrasite), diffuse replacement by a secondary phase (lacroixite), not always resolvable even with backscattered electron imaging, can produce very different light emission response compared to pristine primary phase. Different generations among primary phases (amblygonite-montebrasite) and secondary replacements (lacroixite, apatite) can also be clearly distinguished using this technique (Fig. 5b). Finally, accessory phases (viitaniemiite, mineral D, Phase F), which are inconspicuous and undistinguishable in optical microscopy, have colourful and bright cathodoluminescence and the technique is therefore very appropriate for the detection and textural analysis of such phases (Fig. $1a_3$ & $1b_3$).

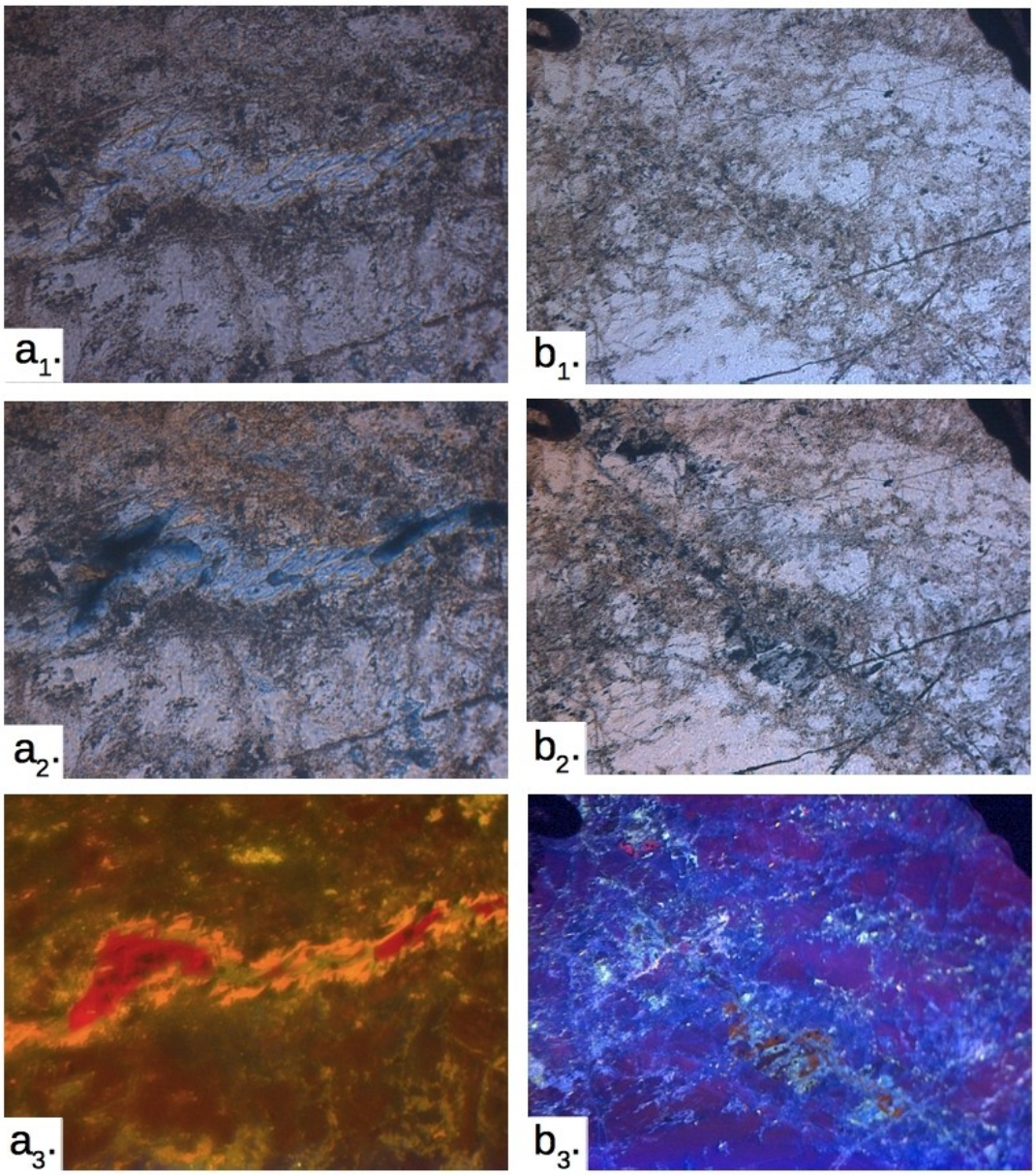

Figure 1. Views of sample MONT2 in plane polarised light (a_1 & b_1), crossed polarised light (a_2 & b_2) and cathodoluminescence in plane-polarised light (a_3 & b_3). Field of view (a) is an assemblage of phase F, lacroixite, amblygonite and kaolinite. Field of view (b) is an assemblage of amblygonite, lacroixite and viitaniemiite. In plane-polarised light (a_1 & b_1), with the exception of relief and some fuzzy alteration features, mineral phases are not exceptionally different. In cross-polars (a_2 & b_2), amblygonite has medium first-order intereference colours, lacroixite is low first order and phase F and viitaniemiite are very low first order. In cathodoluminescence, phase F is crimson red (a_3 & b_3), viitaniemiite is mildy bright orange (b_3), lacroixite has two generations of yellow and blue-green colours (a_3 & b_3) and amblygonite is either dark red brown (a_2) or dark purple (b_2). Kaolinite is not sufficiently luminescent to be visible in this picture.

3.2. Trace element analysis of aluminium phosphates

Trace element data was obtained using a laser ablation inductively coupled plasma mass spectrometry (LA-ICP-MS) at the Research School of Earth Science (RSES, ANU), using a pulsed 193 mm ArF Excimer laser with 3-7 mJ of output energy reaching the sample at a repetition rate of 5 Hz (Eggins et al., 1998), coupled to an Agilent HP7500 quadrupole ICP-MS system. Laser sampling was perfomed in an Ar atmosphere with He:H_2 (ratio 15:1) as a carrier gas with a beam size of 30-50 μm in diameter. ^{27}Al was the internal standard and NIST SRM 612 glass an external standard with reference from Spandler et al. (2011). BCR-2G glass was used as a secondary standard and reproductibility was better than 7%.

LA-ICP-MS analyses were done for amblygonite-montebrasite and lacroixite. Results show the ability of this technique to differentiate between generation of minerals, in agreement with cathodoluminescence, some optical observations and chemical analyses. However, most materials in this study were hardly adequate for this technique as many, seemingly clear, primary amblygonite-montebrasite show contamination from solid and/or fluid inclusions and requires a case-by-case processing of the original signal using GLITTER (Griffin *et al.*, 2008). A comparison with naturally clean analyses with processed data of complex signals show a relatively good removal of contaminants.

In the scope of this paper, the interpretation of trace element data is limited but a more complete study of associated silicates and oxides could provide useful information about the relationship between phosphates parageneses and host rock.

4. Mineral characterisation

4.1. Li-bearing phosphates

Amblygonite-Montebrasite series - *$LiAl(PO_4)(F,OH)$*

This mineral series is the dominant primary phase in phosphate assemblages. It occurs as light-coloured centimetre-sized (or larger) masses ranging from colourless to white, greenish blue or lilac hues. It frequently occurs as idiomorphic crystals but is often altered by quartz, lacroixite, apatite and hydrous phosphates. Fresh amblygonite-montebrasite appears light grey while more altered zones are whiter and seemingly less transparent. Primary amblygonite (Fig. 2a) is often replaced by secondary montebrasite (rarely amblygonite) in lamellae along cleavage and twinning planes and cracks and sometimes requires a careful observation to distinguish twinning from different generations. An occasional late generation of tertiary montebrasite is observed in veins (Fig. 2b).

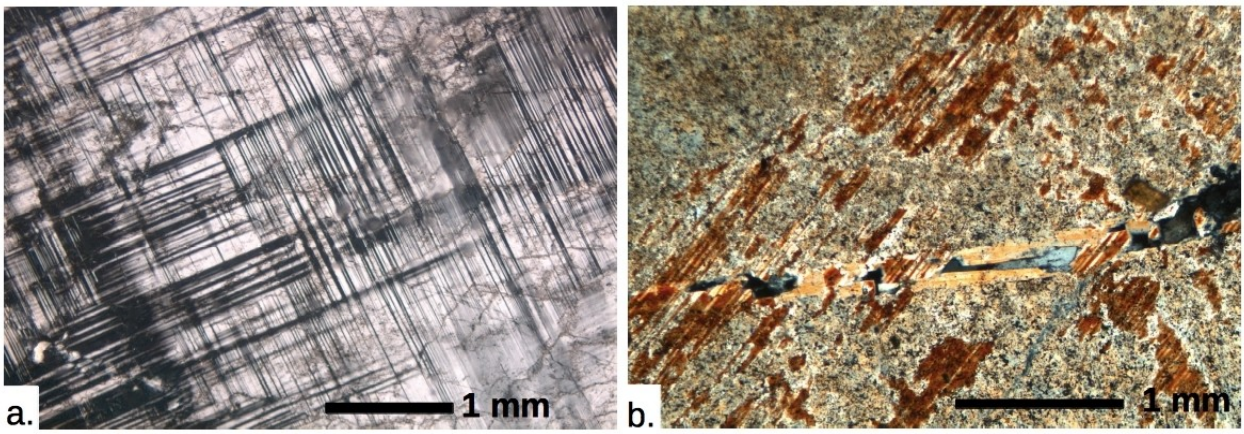

Figure 2. a. Fresh primary amblygonite with chessboard twinning in XPL (sample MONT3). b. Primary amblygonite with replacement along cleavages by secondary amblygonite in XPL. Both amblygonite generations are crosscut by a quartz vein with subiodiomorphic tertiary montebrasite growth (sample MONT9).

Electron probe micro-analysis (EPMA) shows that the primary amblygonite is high in fluorine (>10 wt.% F) while secondary montebrasite range from 6 to 3 wt.% F (Fig. 3). Veinlets of tertiary montebrasite crossing through first and second generation of amblygonite-montebrasite contains hydroxyl-rich montebrasite (below 1 wt.% F; Table 2). Na_2O content in all amblygonite-montebrasite is below <0.1 wt. % and higher values are clearly correlated with lacroixite contamination as observed in CL imaging (Fig. 5b). Cathodoluminescence for amblygonite-montebrasite is weak with little variation between generations. However, there are variation between samples, ranging from blue luminescence (489 to 498 nm) to red luminescence (655 nm) (Fig. $1a_3$, $1b_3$, 5b).

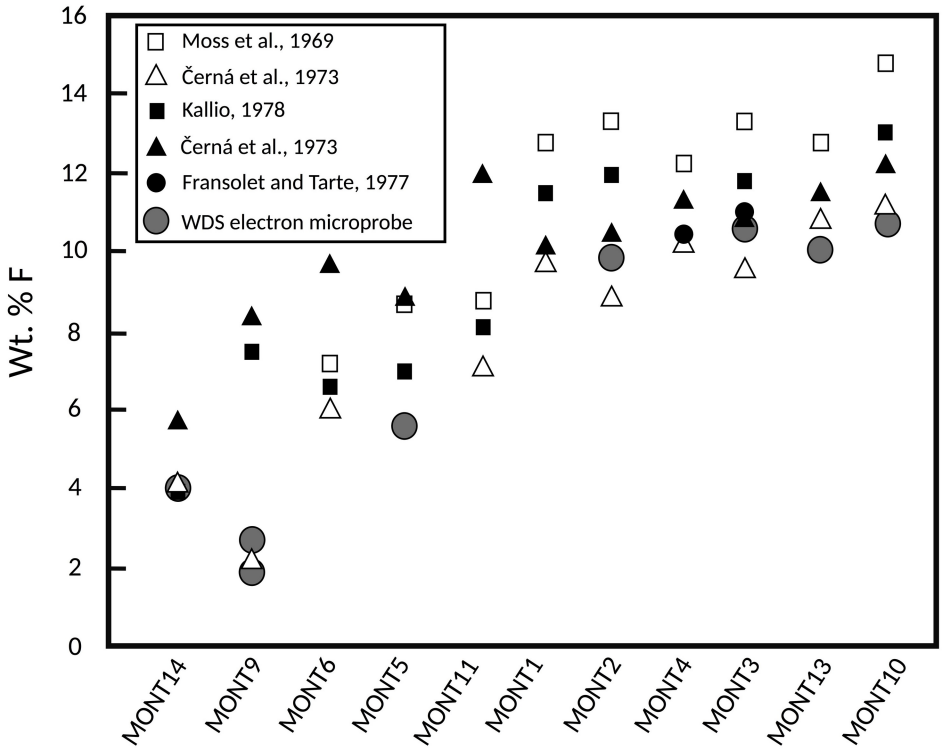

Figure 3. Fluorine determination in bulk amblygonite-montebrasite in different samples by infrared spectroscopy (Fransolet & Tarte, 1977); X-ray diffraction (Moss et al., 1969; Černá et al. 1973; Kallio, 1978) and point analyses with EPMA.

Table 2. Composition of amblygonite-montebrasite

Sample	MONT2	MONT2	MONT3	MONT5	MONT9	MONT9	MONT9	MONT10	MONT10	MONT10	MONT13	MONT14	MONT15	MONT15	ML19
phase	I	II			I	II	III						I	II	
n	7	4	6	6	3	7	3	8	6	3	4	6	1	4	8
P_2O_5	49.22 (43)	49.83 (104)	49.95 (39)	50.79 (60)	50.17 (31)	49.44 (105)	50.79 (104)	50.04 (63)	49.59 (43)	50.18 (45)	50.20 (65)	50.22 (70)	49.97	49.92 (148)	46.02 (68)
Al_2O_3	34.42 (20)	34.45 (35)	34.67 (5)	34.89 (14)	34.32 (13)	34.78 (50)	34.51 (33)	34.86 (26)	34.44 (16)	35.13 (20)	34.75 (15)	35.27 (19)	34.74	34.97 (18)	31.64 (89)
Na_2O	0.80 (70)	1.44 (90)	tr.	bdl	bdl	bdl	bdl	0.11 (6)	0.13 (6)	0.11 (2)	bdl	tr.	bdl	bdl	bdl
F	9.90 (42)	6.59 (143)	10.64 (20)	5.64 (69)	3.63 (30)	1.77 (19)	0.78 (12)	10.69 (9)	9.52 (52)	5.88 (58)	10.03 (50)	4.00 (48)	10.42	4.60 (46)	3.29 (39)
Li_2O	9.87 (39)	9.65 (57)	10.35 (7)	10.49 (11)	10.36 (3)	10.31 (17)	10.47 (15)	10.36 (8)	10.25 (8)	10.41 (8)	10.41 (8)	10.42 (12)	10.39	10.41 (20)	9.52 (19)
H_2O	1.49 (20)	3.11 (75)	1.21 (7)	3.67 (34)	4.53 (13)	5.38 (13)	5.94 (9)	1.21 (7)	1.70 (24)	3.52 (27)	1.53 (21)	4.43 (23)	1.33	4.09 (26)	4.19 (26)
Total	105.70 (43)	105.06 (89)	106.89 (60)	105.53 (70)	103.04 (35)	101.71 (158)	102.49 (147)	107.27 (54)	105.62 (63)	105.23 (78)	106.95 (103)	104.47 (80)	106.84	(0) 104.00 (187)	94.69 (160)
Total O =F	101.53 (41)	102.29 (116)	102.41 (53)	103.16 (62)	101.51 (27)	100.97 (157)	102.16 (144)	102.77 (55)	101.61 (49)	102.76 (68)	102.73 (88)	102.79 (74)	102.46	102.06 (188)	93.30 (168)
P	1.01 (0)	1.01 (1)	1.01 (0)	1.02 (1)	1.02 (0)	1.01 (1)	1.02 (1)	1.01 (1)	1.01 (0)	1.01 (0)	1.01 (0)	1.01 (1)	1.01	1.01 (1)	1.02 (1)
Al	0.98 (1)	0.98 (1)	0.98 (0)	0.97 (1)	0.97 (1)	0.99 (1)	0.97 (1)	0.98 (1)	0.98 (1)	0.98 (1)	0.98 (1)	0.99 (1)	0.98	0.98 (2)	0.97 (1)
Na	0.04 (3)	0.07 (4)	tr.	bdl	bdl	bdl	bdl	0.01 (0)	0.01 (0)	0.01 (0)	bdl	tr.	bdl	bdl	bdl
F	0.76 (3)	0.50 (11)	0.81 (1)	0.42 (5)	0.27 (2)	0.14 (1)	0.06 (1)	0.81 (1)	0.73 (4)	0.44 (4)	0.76 (3)	0.30 (4)	0.79	0.35 (4)	0.27 (4)
Li	0.96 (3)	0.93 (4)	1.00 (0)	1.00 (1)	1.00 (0)	1.00 (0)	1.00 (0)	0.99 (0)	0.99 (0)	0.99 (0)	1.00 (0)	0.99 (1)	1.00	1.00 (0)	1.00 (0)
OH	0.24 (3)	0.50 (11)	0.19 (1)	0.58 (5)	0.73 (2)	0.86 (1)	0.94 (1)	0.19 (1)	0.27 (4)	0.56 (4)	0.24 (3)	0.70 (4)	0.21	0.65 (4)	0.73 (4)
Σcat.	2.99 (0)	2.99 (0)	2.99 (0)	2.99 (0)	2.99 (0)	2.99 (1)	2.99 (0)	2.99 (0)	2.99 (0)	2.99 (0)	2.99 (0)	2.99 (0)	2.99	2.99 (1)	2.99 (1)
F/(F+OH)	0.76 (3)	0.50 (11)	0.81 (1)	0.42 (5)	0.27 (2)	0.14 (1)	0.06 (1)	0.81 (1)	0.73 (4)	0.44 (4)	0.76 (3)	0.30 (4)	0.79	0.35 (4)	0.27 (4)

Amblygonite-Montebrasite calculated on 4 oxygens - Hydroxyls calculated by difference on fluorine site (1-F) - Li calculated by difference of Na on lithium site (1-Na)

Trace elements contents in primary and secondary amblygonite-montebrasite have similar ranges and only display rare differences (Fig. 4). Although Al^{3+} in montebrasite is known to allow substitution with trivalent and tetravalent cations (Dias et al., 2011), most anomalies and variability between trace elements concentrations seem to be linked to the presence of micro-inclusions, as it is known in such phosphates (Shirose & Uehara, 2014). Veinlets of tertiary montebrasite, which are more transparent, have smoother trace elements patterns and display a clear enrichment in medium rare earth elements (REE) over light and heavy REE as well as an enrichment in alkalis and transitions metals.

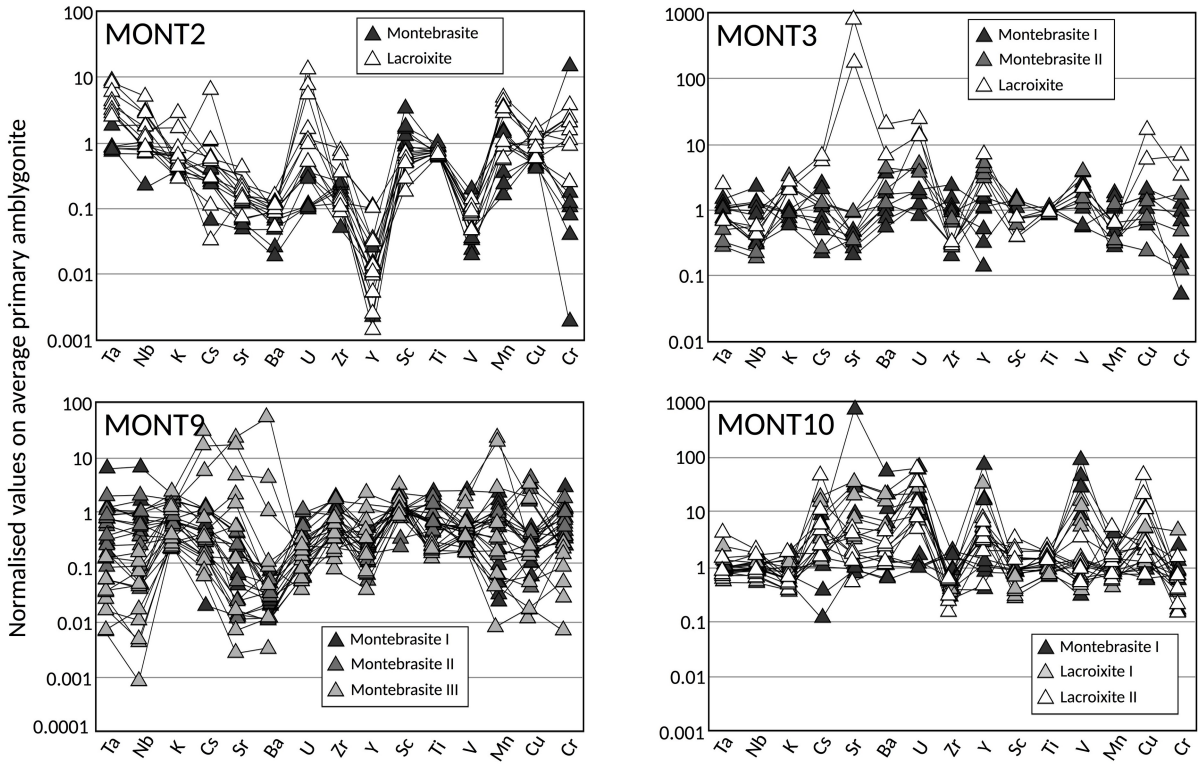

Figure 4. Trace element concentration in amblygonite-montebrasite and lacroixite normalised on the associated average primary amblygonite free of any inclusions. Variations are mostly systematic within samples but varies between samples.

4.2. Na-bearing phosphates

Lacroixite – *$NaAlPO_4F$*

Lacroixite is present in all samples as a diffuse alteration of amblygonite-montebrasite occurring as a micron-size mesh and occasionally showing submillimetre whitish veinlets (Fig. 5a). Optical microscopy observations remain difficult due to the submicroscopic meshy texture and similar optical properties with amblygonite that lead to the erroneous identification of natromontrebasite in many pegmatites (Fransolet et al., 2007). In the studied samples, cathodoluminescence is a very powerful tool to identify lacroixite in amblygonite (Fig. 1b$_3$, 5b). Early lacroixite has a yellow-green luminescence (549 nm) while later lacroixite has a blue-greenish luminescence (487 to 513 nm), contrasting with duller background colours of amblygonite-montebrasite. Occasionally, secondary euhedral lacroixite grows on vein walls, reaching up to ~100 μm in length and is often associated with fluorapatite and phase F.

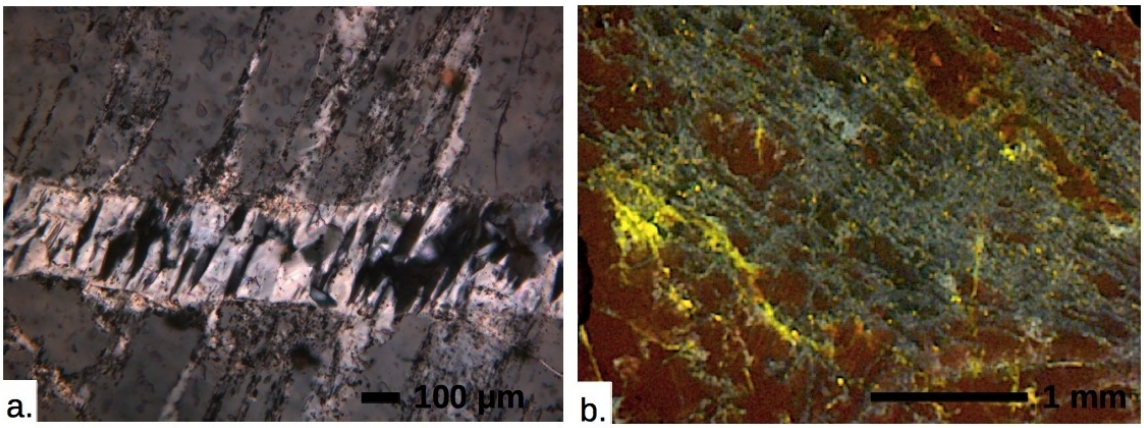

Figure 5. a. Lacroixite veinlet with crystal growth aligned with cleavage of surrounding primary amblygonite in XPL (Sample MONT 10). b. Two generation (yellow & blue) of meshy lacroixite in primary amblygonite (dark red). Lacroixite replacement zones have a vague alignment with amblygonite cleavages in CL-PPL (Sample MONT 2).

X-ray diffraction and EPMA of lacroixite provide chemical data near the ideal composition with a weak positive correlation between Na/(Na+Li) and F/(F+OH) (Table 3). Trace elements in meshy

lacroixite show a non-systematic enrichment in U, Sr, Ba, Cs, Cu and Cr while lacroixite veins mostly show Cu, Cs and U as enriched elements and slightly depleted in other elements compared to the primary amblygonite (Fig. 4).

Table 3. Composition of lacroixite

Sample	MONT2-a	MONT2-b	MONT2-c	MONT2-d	MONT2-UCL	MONT2-UCL	MONT3-a	MONT10-a	MONT10-UCL	MONT13-a	MONT20-a
phase	blue CL	yellow CL	cream CL				vein				
n	9	3	3	3	unk	unk	6	8	unk	2	5
P_2O_5	41.30 (14)	40.27 (63)	43.94 (23)	42.91 (148)	42.07 (195)	40.87 (159)	42.25 (179)	43.05 (80)	41.01 (104)	44.06 (93)	44.87 (69)
Al_2O_3	31.77 (11)	32.13 (17)	31.22 (33)	31.70 (56)	31.31 (21)	31.04 (45)	31.44 (26)	31.48 (64)	31.49 (14)	31.72 (95)	31.17 (34)
Na_2O	18.41 (22)	18.54 (5)	18.03 (14)	18.11 (19)	16.24 (136)	16.57 (206)	17.74 (74)	17.74 (74)	17.51 (51)	15.16 (75)	15.79 (86)
F	13.15 (263)	18.24 (74)	12.81 (47)	14.83 (215)	12.71 (257)	13.42 (292)	15.21 (108)	11.35 (43)	13.57 (37)	10.46 (31)	11.63 (53)
Li_2O	tr.	bdl	0.46 (9)	0.36 (19)	1.05 (81)	tr.	1.00 (59)	0.51 (35)	0.37 (18)	1.80 (55)	1.56 (45)
Total	104.70 (318)	109.18 (36)	106.46 (79)	107.90 (132)	103.37 (119)	102.68 (248)	106.29 (143)	104.14 (296)	103.95 (93)	103.21 (137)	105.02 (103)
Total O =F	99.16 (301)	101.50 (43)	101.07 (65)	101.66 (53)	98.02 (55)	97.03 (166)	99.88 (151)	99.36 (282)	98.24 (107)	98.80 (150)	100.12 (95)
P	0.97 (0)	0.96 (1)	1.01 (0)	0.99 (2)	1.00 (3)	0.99 (3)	1.00 (2)	1.00 (2)	0.98 (1)	1.02 (0)	1.03 (1)
Al	1.04 (0)	1.06 (1)	1.00 (1)	1.02 (3)	1.04 (2)	1.05 (2)	1.04 (2)	1.02 (2)	1.05 (2)	1.03 (1)	1.00 (1)
Na	1.00 (1)	1.01 (1)	0.95 (1)	0.96 (2)	0.89 (9)	0.92 (11)	0.89 (6)	0.94 (4)	0.96 (2)	0.81 (5)	0.83 (5)
F	1.16 (23)	1.62 (8)	1.10 (4)	1.29 (20)	1.13 (25)	1.22 (28)	1.35 (12)	0.99 (4)	1.21 (5)	0.91 (4)	1.00 (5)
Li	tr.	bdl	0.05 (1)	0.04 (2)	0.11 (9)	tr.	0.11 (6)	0.06 (4)	0.04 (2)	0.19 (5)	0.17 (5)
Σcat.	3.02 (0)	3.03 (1)	3.01 (0)	3.02 (1)	3.04 (1)	3.04 (2)	3.04 (1)	3.02 (1)	3.03 (1)	3.05 (2)	3.03 (1)
F/(F+OH)	1.00 (0)	1.00 (0)	1.00 (0)	1.00 (0)	0.96 (9)	1.00 (1)	1.00 (0)	0.99 (2)	1.00 (0)	0.91 (4)	0.98 (2)

Lacroixite calculated on 9 electrical charges - Hydroxyls calculated by difference on fluorine site (1-F) - Li calculated by difference of Na on sodium site (1-Na)
Samples MONT2-a and MONT10 are measured with time-zero integrated analysis

Wardite –$NaAl_3(PO_4)_2(OH)_4 \bullet 2H_2O$

Wardite has been observed and identified through X-ray and EPMA. It occurs in alteration zones of quartz veins containing wavellite, variscite, turquoise and apatite. Important or complete replacement by apatite is common (Fig 6b). Chemical composition of wardite in Montebras is $(Na_{0.94}Ca_{0.04}Mg_{0.01})Al_{2.95}(PO_4)_{2.05}(OH_{3.57}F_{0.37}) \bullet 2H_2O$ (Table 4).

Table 4. Composition of wardite, morinite and viitaniemiite

Sample	MONT9	MONT12	MONT12	MONT12	MONT12	MONT2	MONT2	MONT5
phase	Wardite	Morinite	Morinite	Morinite	Morinite	Viitaniemiite	Viitaniemiite	Viitaniemiite
n	9	6	17	6	15	8	6	8
P_2O_5	36.10 (46)	28.14 (206)	28.27 (141)	29.74 (79)	29.46 (76)	30.28 (118)	27.66 (46)	29.65 (63)
Al_2O_3	37.27 (76)	21.26 (49)	21.01 (74)	21.15 (58)	20.59 (51)	21.92 (60)	21.76 (15)	20.16 (17)
FeO	*n.a.*	*n.a.*	*n.a.*	*n.a.*	*n.a.*	tr.	tr.	1.30 (36)
MgO	0.13 (8)	*n.a.*	*n.a.*	*n.a.*	*n.a.*	2.21 (38)	0.10 (2)	0.08 (4)
MnO	*n.a.*	*n.a.*	*n.a.*	*n.a.*	*n.a.*	3.42 (29)	2.25 (42)	14.05 (101)
CaO	0.52 (53)	22.42 (49)	22.33 (52)	22.72 (20)	22.79 (47)	16.89 (129)	21.70 (70)	9.67 (118)
Na_2O	7.24 (35)	3.69 (28)	4.96 (27)	5.89 (19)	6.15 (15)	12.90 (28)	11.79 (16)	12.07 (44)
F	0.79 (17)	14.56 (56)	16.23 (92)	16.74 (160)	17.19 (99)	17.41 (72)	19.56 (61)	15.33 (62)
H2O	17.56 (71)	15.89 (327)	13.80 (258)	10.19 (189)	10.37 (145)	3.16 (38)	1.66 (20)	3.57 (36)
Total	99.61 (37)	105.96 (120)	106.60 (68)	106.44 (56)	106.56 (58)	108.22 (137)	106.50 (112)	106.04 (127)
Total O =F	99.28 (36)	99.83 (112)	99.77 (53)	99.38 (47)	99.32 (56)	100.89 (121)	98.26 (86)	99.58 (133)
P	2.05 (2)	2.00 (8)	2.00 (4)	2.03 (3)	2.02 (3)	1.01 (2)	0.96 (1)	1.04 (1)
Al	2.94 (5)	2.11 (10)	2.06 (6)	2.00 (7)	1.97 (4)	1.02 (1)	1.05 (1)	0.99 (2)
Fe	*n.a.*	*n.a.*	*n.a.*	*n.a.*	*n.a.*	tr.	tr.	0.05 (1)
Mg	0.01 (1)	*n.a.*	*n.a.*	*n.a.*	*n.a.*	0.13 (2)	0.01 (0)	0.01 (0)
Mn	*n.a.*	*n.a.*	*n.a.*	*n.a.*	*n.a.*	0.11 (1)	0.08 (2)	0.49 (3)
Ca	0.04 (4)	2.02 (5)	1.99 (4)	1.96 (2)	1.98 (4)	0.71 (6)	0.96 (3)	0.43 (5)
Na	0.94 (5)	0.60 (5)	0.80 (3)	0.91 (2)	0.97 (2)	0.98 (1)	0.94 (1)	0.97 (3)
F	0.17 (4)	3.79 (11)	4.00 (8)	3.97 (15)	4.19 (12)	2.17 (9)	2.54 (6)	2.01 (9)
OH	3.83 (4)	1.21 (11)	1.00 (8)	1.03 (15)	0.81 (12)	0.83 (9)	0.46 (6)	0.99 (9)
H2O	2.01 (19)	3.93 (118)	3.45 (94)	2.41 (42)	2.49 (40)	*n.a.*	*n.a.*	*n.a.*
Σcat.	5.99 (3)	6.75 (7)	6.88 (5)	6.92 (2)	6.98 (4)	3.98 (4)	4.00 (2)	3.98 (2)
F/(F+OH)	0.04 (1)	0.76 (2)	0.80 (2)	0.79 (3)	0.84 (2)	0.72 (3)	0.85 (2)	0.67 (3)

Wardite calculated on 20 electrical charges - Hydroxyls calculated by difference on hydroxyl site (4-F)
Morinite calculated on 21 electrical charges - Hydroxyls calculated by difference on fluorine site (5-F)
Viitaniemiite calculated on 11 electrical charges - Hydroxyls calculated by difference on fluorine site (3-F)
H2O calculated by difference on total measured and calculated hydroxyls groups

4.3. Na-Ca-bearing phosphates

Morinite – $NaCa_2Al_2(PO_4)_2(F,OH)_5 \bullet 2H_2O$

Montebras is the type locality of morinite (Lacroix, 1891). It occurs as purple-red masses and fibrous crusts with concentric colour changes. Samples available for this study show morinite as a filling in a late quartz vein with no amblygonite present, in contrast with the original description of this mineral in amblygonite geodes (Lacroix, 1891; Lahti, 1981). Minerals associated with morinite are crandallite, turquoise and a replacement by apatite (Fig. 6c). Some samples have mineral phases visually similar to morinite but further analysis (cathodoluminescence, EPMA) showed these to be a fibrous sodium-bearing apatite (Fig. 6e).

Cathodoluminescence is not very intense but clear zonation growth is visible with pink, orange and brown colours appearing in crusts (Fig. 6d). EPMA analyses show a decrease in sodium (1.0 to 0.67 Na.p.f.u.) from the inside to the outside of morinite crusts. Average composition is $Na_{0.94}Ca_{1.97}Mg_{0.01}Al_{1.97}(PO_4)_{2.04}(F_{4.26}OH_{0.43}) \bullet 2H_2O$ (Table 4). Substitutions mentioned by Čech and Povondra (1985) have not been observed in these samples.

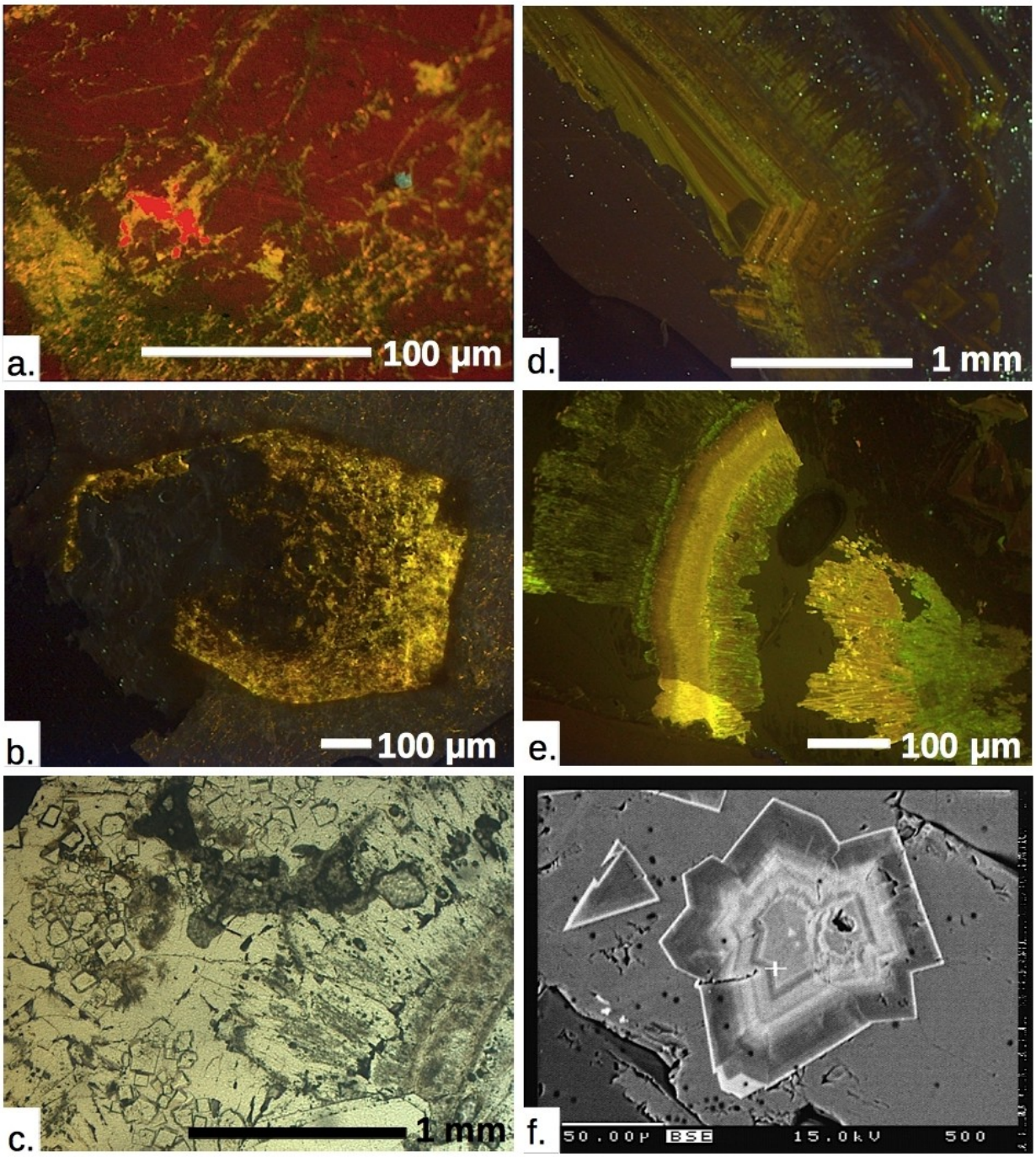

Figure 6. a. Viitaniemiite (bright red) in primary and secondary amblygonite (dark red) altered by lacroixite (greenish yellow) in CL-PPL (Sample MONT2) b. Sodium-rich apatite pseudomorph of an euhedral wardite crystal in a quartz vein in CL-PPL. (Sample MONT3). c. Morinite crust with replacement by euhedral crystals of crandallite-goyazite and some apatite in PPL (Sample MONT 12). d. Morinite crystal with internal zoned textures in a quartz vug in CL-PPL (Sample MONT12). e. Fibrous sodium-rich apatite pseudomorph of a morinite crust preserving some of the original zonation in CL-PPL (Sample MONT12). f. Euhedral crystal of the complete solid solution between crandallite (dark grey) and goyazite (light grey) in morinite in BSE (Sample MONT12).

Viitaniemiite – *$Na(Ca,Mn)Al(PO_4)(F,OH)_3$*

Viitaniemiite is a rare mineral that occurs in Montebras as a colourless phase in altered amblygonite. It is pervasively mixed with lacroixite as rare patches of a couple of hundred microns. Viitaniemiite is recognisable in cathodoluminescence with a brown-orange (Fig. $1a_3$) to red colour of medium intensity (Fig. 6a). Studies on doped synthetic viitaniemiite suggest that REE and Mn^{2+} could be responsible for such hue (Nagaraja et al., 2017; Pushpa Manjari et al., 2014). EPMA shows a Mn-Mg-bearing viitaniemiite with the following composition: $Na_{0.93}(Ca_{0.82}Mn_{0.09}Mg_{0.07})Al_{1.03}(PO_4)_{0.99}(F_{2.30}OH_{0.72})$ (Table 4). Changes in cathodoluminescent colours can be correlated with Ca ⇔ Mn,Mg exchange and $2Na^+$ ⇔ $(Ca,Mn,Mg)^{2+}$ (Shirose & Uehara, 2014; Petrík et al., 2011; Lathi, 1981). The first substitution leads to a viitaniemiite where manganese is more abundant than calcium (Fig. 7).

Mineral D – *$Na(Mn,Ca)Al(PO_4)(F,OH)_3$*

Although similar in composition to viitaniemiite, this mineral phase was found in a different assemblage as a low relief and very low birefringence phase in eosphorite as inclusions up to 250 *μm*. Textures seem to indicate that it is an alteration product of eosphorite.

Microprobe analysis gives $Na_{0.96}(Mn_{0.49}Ca_{0.42}Fe_{0.04}Mg_{0.01})Al_{0.97}(PO_4)_{1.03}(F_{1.98}OH_{0.73})$ (Table 4). This composition seems to be part of a viitaniemiite solid solution involving the substitution Ca^{2+} ⇔ $(Mn, Fe, Mg)^{2+}$ (Fig. 7) only partly evidenced in a Carpathians quartz vein (Stevko et al., 2015) and in Namibia (Pirard, 2022).

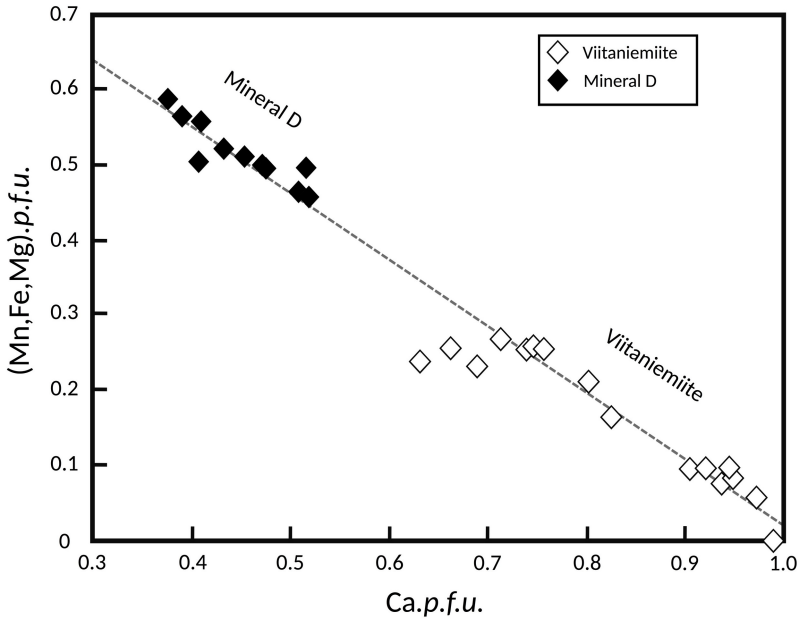

Figure 7. Evidence of substitution Ca <=> Mn+Fe+Mg in viitaniemiite-like minerals of Montebras.

4.4. Ca-bearing phosphates

Fluorapatite – $Ca_5(PO_4)_3F$

Apatite is a frequent mineral that seems to occur at all post-magmatic stages of crystallisation and hydrothermal alteration, as euhedral crystals, veins (with quartz and lacroixite), radiating masses or microscopic inclusions in montebrasite, crandallite, cassiterite, wavellite and turquoise. Apatite has a very bright cathodoluminescence in orange-yellow to yellow greenish hues (545 to 580 nm) (Fig. 6b, 6e).

X-ray diffraction, infrared data and EPMA clearly show that apatites are invariably near the F-rich end-member. Manganese content ranges from 0.4 to 3 wt.% MnO while iron rarely reaches 0.4 wt.% FeO. Apatite associated with morinite and wardite have up to 1 wt.% Na_2O and 0.5 wt.% Al_2O_3 (Table 5).

Table 5. Composition of apatite

Sample *phase* n	MONT9 9	MONT9 brown CL 5	MONT9 3	MONT9 2	MONT12 4	MONT12 10	MONT12 8
P_2O_5	41.96 (111)	41.88 (89)	41.49 (130)	43.39 (24)	42.14 (54)	40.18 (83)	40.78 (77)
Al_2O_3	tr.	0.13 (10)	tr.	bdl	0.11 (5)	0.17 (11)	0.22 (15)
FeO	0.34 (27)	0.33 (10)	0.36 (0)	tr.	0.10 (8)	tr.	tr.
MnO	2.99 (64)	1.24 (36)	1.93 (25)	0.77 (8)	1.04 (54)	0.43 (45)	0.44 (35)
CuO	bdl	bdl	bdl	bdl	0.17 (11)	bdl	bdl
CaO	51.58 (120)	53.44 (130)	52.39 (62)	53.13 (67)	52.84 (48)	53.80 (104)	53.49 (122)
SrO	*n.a.*	*n.a.*	*n.a.*	*n.a.*	*n.a.*	*n.a.*	0.01 (3)
Na_2O	bdl	bdl	bdl	bdl	0.19 (11)	0.41 (35)	tr.
F	3.56 (30)	4.26 (38)	2.52 (60)	4.64 (20)	4.61 (26)	4.06 (24)	4.33 (77)
H2O							
Total	100.47 (135)	101.12 (89)	98.71 (78)	102.07 (99)	101.19 (62)	99.07 (147)	99.42 (166)
Total O =F	98.97 (138)	99.32 (95)	97.65 (103)	100.12 (91)	99.25 (58)	97.37 (148)	97.60 (137)
P	3.03 (5)	3.00 (3)	3.01 (4)	3.07 (1)	3.03 (2)	3.00 (4)	2.98 (3)
Al	tr.	0.02 (1)	tr.	tr.	tr.	tr.	0.02 (1)
Fe	tr.	bdl	tr.	bdl	tr.	bdl	bdl
Mn	0.22 (5)	0.09 (2)	0.14 (2)	0.05 (1)	0.07 (4)	0.04 (2)	tr.
Cu	bdl	bdl	bdl	bdl	bdl	0.01 (0)	bdl
Ca	4.71 (10)	4.89 (8)	4.82 (11)	4.76 (2)	4.81 (5)	4.96 (11)	5.03 (8)
Sr							
Na	tr.	tr.	0.01 (0)	0.01 (0)	0.05 (2)	0.07 (4)	0.13 (3)
F	0.96 (8)	1.03 (2)	0.69 (18)	1.23 (4)	1.24 (7)	1.11 (9)	1.12 (7)
OH	0.06 (6)	bdl	0.31 (18)	0.17 (468)			
Σcat.	8.00 (6)	8.02 (2)	8.02 (8)	3.03 (101)	8.02 (5)	8.10 (4)	8.19 (4)
F/(F+OH)	0.96 (0)	1.00	0.69	1.00	0.96	1.00	1.00

Apatite calculated on 25 electrical charges - Hydroxyls calculated by difference on fluorine site (1-F)

Crandallite-Goyazite – $(Ca,Sr)Al_3(PO_4)_2(OH)_5 \bullet H_2O$

Crandallite group minerals are a common alteration phase and show extensive substitution in the Ca-Sr-Ba-REE space. Barium-poor crandallite and goyazite are very common and occur as veinlets associated with most other phosphates. Morinite crusts have numerous zoned euhedral rhombohedra of Ba-free crandallite-goyazite (Fig. 6c).

Crandallite group minerals are not cathodoluminescent, probably as a result of the absence of manganese and up to 1 wt.% FeO that would act as a luminescence quencher. The distribution of crandallite group mineral compositions show a complete solid solution between Ca and Sr (Fig. 6f) while the substitution towards Ba is limited (less than 6% of the divalent site) (Fig. 8b). This observation could confirm the existence of the interval of insolubility between Sr and Ba suggested by Liferovich *et al.* (1999) and not the complete solid solution hypothesised elsewhere (Baldwin et al., 2000) (Table 6).

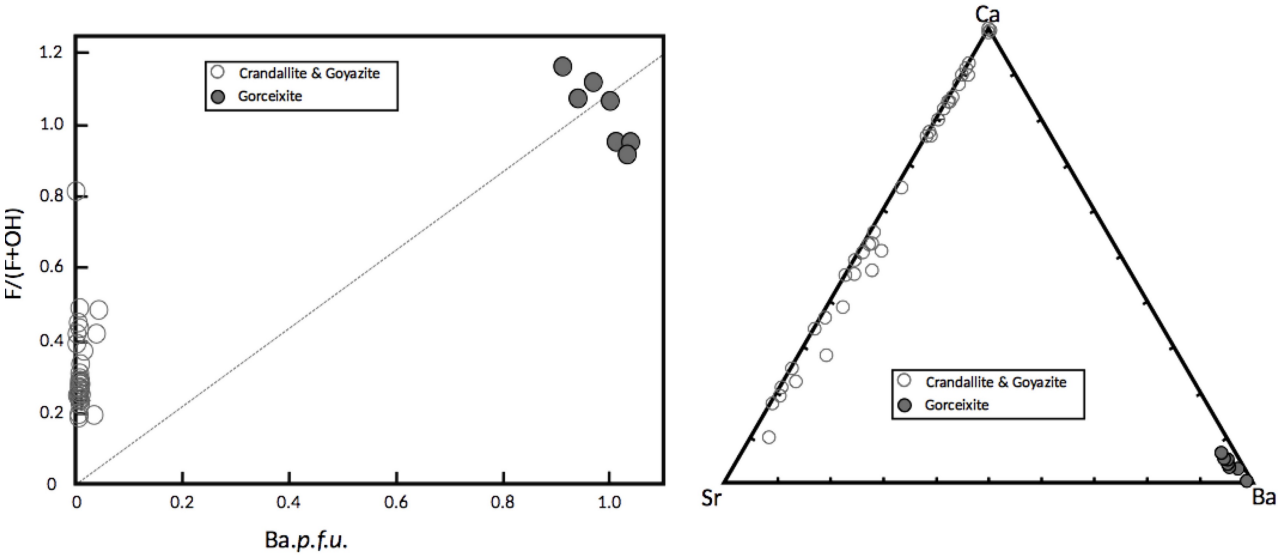

Figure 8. a. Distribution of crandallite-goyazite and gorceixite as a function of fluorine content. b. Distribution of crandallite group mineral as a propportion of Ca, Sr and Ba.

Gorceixite – $BaAl_3(PO_4)(PO_3OH)(OH)_6 \bullet H_2O$

Gorceixite occurs in more heavily altered zones than crandallite-goyazite, associated with kaolinite where it forms cryptocrystalline crusts. The average composition obtained for this mineral is $(Ba_{0.97}Ca_{0.04}Sr_{0.02})Al_{2.96}Fe_{0.05}(PO_4)(PO_3OH)F_{1.04}(OH)_{5.95} \bullet 1.53H_2O$ (Table 6). The high fluorine content is a common feature of gorceixite and also seen in the nearby locality of Echassieres (Nicolas & de Rosen, 1963) and in several other places (Taylor et al., 1984; Milton et al., 1958;

White 1981; Pirard, 2022). A possible mechanism supporting this observation is $(Ca,Sr)^{2+} + OH^{-}$ <=> $Ba^{2+} + F^{-}$ although more data would be required to validate this substitution (Fig. 8).

Table 6. Composition of crandallite group minerals

Sample	MONT7	MONT7	MONT9	MONT12	MONT12	MONT12	MONT12	MONT12	MONT12
phase	Gorceixite	Gorceixite	Goyazite	Crandallite	Crandallite	Goyazite	Crandallite	Goyazite	Goyazite
n	5	3	3	5	7	3	4	5	2
P_2O_5	25.78 (26)	26.33 (49)	32.55 (98)	29.40 (43)	27.76 (143)	27.40 (327)	29.22 (284)	23.48 (102)	26.77 (85)
Al_2O_3	27.73 (15)	27.38 (30)	32.65 (77)	34.06 (33)	35.56 (61)	32.42 (111)	37.54 (444)	31.96 (129)	33.22 (45)
FeO	0.59 (21)	0.85 (66)	bdl	bdl	bdl	bdl	bdl	bdl	0.04 (1)
MnO	bdl	bdl	bdl	bdl	bdl	0.13 (12)	bdl	bdl	bdl
CuO	0.17 (4)	0.08 (4)	bdl	0.13 (5)	bdl	0.06 (3)	bdl	0.07 (3)	0.14 (11)
CaO	0.58 (9)	0.26 (19)	5.64 (77)	6.58 (42)	11.04 (45)	3.37 (196)	12.90 (101)	2.68 (48)	5.58 (30)
SrO	0.52 (3)	0.32 (22)	11.57 (159)	10.99 (53)	3.34 (168)	15.98 (145)	0.63 (126)	18.10 (32)	12.00 (99)
BaO	26.72 (91)	28.68 (25)	1.31 (26)	0.28 (18)	bdl	bdl	bdl	0.19 (24)	bdl
Na_2O	0.07 (2)	0.09 (3)	bdl	0.04 (3)	bdl	0.01 (0)	bdl	bdl	0.03 (1)
K_2O	0.22 (5)	0.11 (8)	bdl	bdl	bdl	bdl	bdl	bdl	bdl
F	3.83 (14)	3.24 (5)	1.56 (68)	1.15 (4)	1.14 (37)	2.34 (219)	1.09 (12)	1.34 (27)	1.30 (25)
H_2O	15.51 (53)	13.74 (124)	14.13 (82)	18.89 (85)	23.79 (300)	20.11 (571)	21.46 (732)	25.74 (162)	23.14 (162)
Total	102.17 (22)	101.71 (32)	99.77 (83)	101.67 (17)	103.00 (55)	102.46 (125)	103.05 (46)	103.78 (77)	102.56 (45)
Total O =F	100.55 (25)	100.35 (33)	99.11 (64)	101.19 (18)	102.52 (68)	101.47 (203)	102.60 (41)	103.21 (73)	102.02 (35)
P	1.99 (2)	2.02 (1)	2.07 (5)	1.92 (1)	1.82 (5)	1.89 (16)	1.82 (1)	1.74 (6)	1.85 (3)
Al	2.98 (2)	2.93 (4)	2.89 (8)	3.10 (4)	3.25 (11)	3.13 (19)	3.26 (6)	3.31 (12)	3.20 (9)
Fe	0.05 (2)	0.06 (5)	bdl	bdl	bdl	bdl	bdl	bdl	0.00 (0)
Mn	bdl	bdl	bdl	bdl	bdl	0.01 (1)	bdl	bdl	bdl
Cu	0.02 (1)	bdl	bdl	bdl	bdl	0.01 (0)	bdl	0.01 (0)	0.02 (1)
Ca	0.06 (1)	0.03 (2)	0.45 (6)	0.54 (3)	0.92 (3)	0.30 (18)	1.02 (2)	0.25 (4)	0.49 (2)
Sr	0.03 (0)	0.02 (1)	0.50 (7)	0.49 (3)	0.15 (7)	0.76 (5)	0.03 (6)	0.92 (2)	0.57 (4)
Ba	0.96 (3)	1.02 (1)	0.04 (1)	bdl	bdl	bdl	bdl	bdl	0.01 (1)
Na	0.01 (0)	0.02 (1)	bdl	0.01 (0)	bdl	bdl	bdl	bdl	0.01 (0)
K	0.03 (1)	bdl	bdl	bdl	bdl	bdl	bdl	bdl	bdl
F	1.11 (4)	0.93 (2)	0.37 (16)	0.28 (1)	0.28 (8)	0.59 (53)	0.25 (1)	0.37 (8)	0.34 (7)
OH	3.89 (4)	4.07 (2)	4.63 (16)	4.72 (1)	4.72 (8)	4.41 (53)	4.75 (1)	4.63 (8)	4.66 (7)
H_2O	2.78 (18)	2.12 (41)	1.23 (27)	2.51 (25)	3.81 (87)	3.32 (147)	3.07 (217)	5.23 (62)	3.98 (56)
Σ(Ca,Sr,Ba)	1.04 (3)	1.06 (4)	1.00 (1)	1.05 (3)	1.07 (8)	1.07 (14)	1.05 (7)	1.18 (5)	1.07 (5)
F/(F+OH)	0.22 (1)	0.19 (0)	0.07 (3)	0.06 (0)	0.06 (2)	0.12 (11)	0.05 (0)	0.07 (2)	0.07 (1)

Crandallite group calculated on 21 electrical charges - Hydroxyls calculated by difference on fluorine site (5-F)
H2O calculated by difference on total measured and calculated hydroxyl groups

4.5. Cation-free aluminium phosphates

Variscite – $AlPO_4 \bullet 2H_2O$

Variscite is a common cryptocrystalline cream-coloured phase forming an intimate mixture with kaolinite, wavellite and quartz on the outer part of most samples (Fig. 9a). It not easily seen under an optical microscope and cathodoluminescence is of no real help to differentiate fine grained mixtures of quartz, wavellite and variscite. In our samples, the occasional green colour of variscite-rich assemblage is rather due to the presence of turquoise and possibly minerals such as barrandite and dufrenite (Lacroix, 1910).

Wavellite – $Al_3(PO_4)_2(OH,F)_3 \bullet 5H_2O$

Wavellite forms characteristic acicular aggregates, crusts and independent needles up to 5 mm long (Fig. 9b). It is associated with many alteration phases and rarely in direct contact with amblygonite. Average chemical composition is $Al_{2.93}Fe_{0.01}(PO_4)_{2.04}(OH_{2.12}F_{0.88}) \bullet 5.04H_2O$ (Table 7).

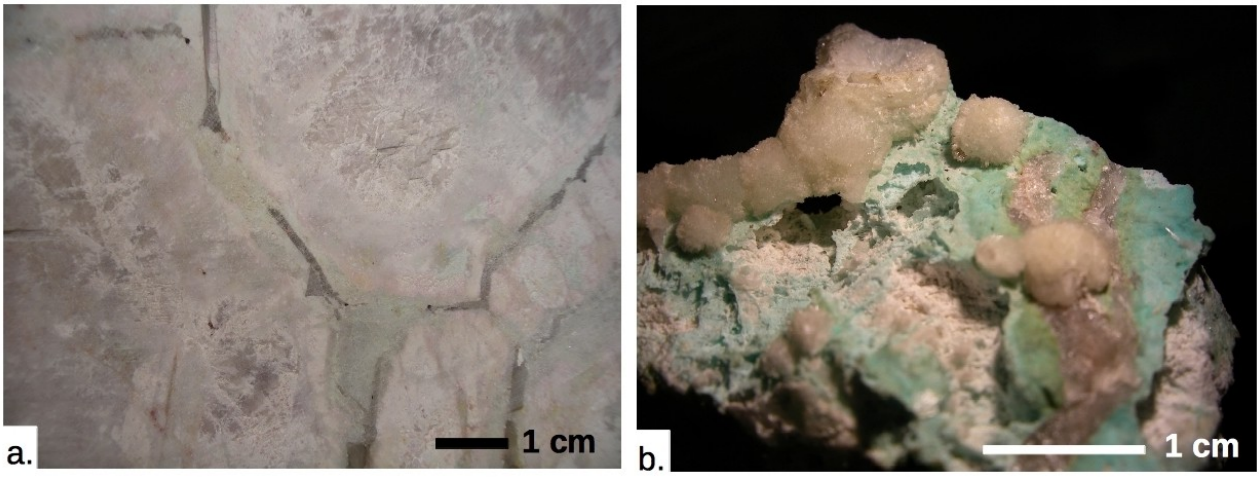

Figure 9. a. Macroscopic view of an alteration zone in amblygonite+lacroixite (light grey) showing quartz veins (grey) surrounded by variscite (greenish) and wavellite (cream) and a wider zone of kaolinization (white) (Sample MONT 13). b. Macroscopic view of an alteration crust over altered (kaolinized) amblygonite with quartz veins (grey), variscite (greenish), turquoise (bluish) and wavellite radiating aggregates (Sample MONT 8).

Table 7. Composition of wavellite and turquoise

Sample	MONT13	MONT15	MONT5	MONT3
phase	Wavellite	Wavellite	Turquoise	Turquoise
n	2	2	3	2
P_2O_5	34.88 (72)	34.58 (67)	33.65 (205)	33.70 (94)
Al_2O_3	35.66 (60)	35.56 (22)	34.66 (140)	34.97 (141)
FeO	0.10 (3)	0.08 (6)	0.09 (7)	2.16 (44)
MnO	*bdl*	0.11 (3)	*n.a.*	*n.a.*
CuO	*bdl*	0.08 (7)	4.36 (259)	5.26 (77)
CaO	0.03 (1)	*bdl*	0.62 (51)	1.21 (83)
Na_2O	*bdl*	*bdl*	bdl	0.57 (48)
K_2O	0.07 (4)	0.15 (3)	0.16 (3)	0.12 (2)
F	3.96 (4)	4.00 (22)	1.11 (28)	2.23 (22)
H_2O	26.05 (71)	26.47 (117)	23.78 (471)	20.25 (23)
Total	100.98 (56)	101.14 (12)	99.51 (130)	100.63 (102)
Total O =F	99.32 (54)	99.46 (21)	99.04 (121)	99.69 (112)
P	2.05 (4)	2.04 (1)	4.17 (17)	4.07 (13)
Al	2.92 (6)	2.93 (2)	5.99 (21)	5.88 (21)
Fe	0.01 (0)	*bdl*	bdl	0.26 (5)
Mn	*bdl*	0.01 (0)	*n.a.*	*n.a.*
Cu	*bdl*	*bdl*	0.47 (26)	0.57 (8)
Ca	*bdl*	*bdl*	0.10 (8)	0.19 (13)
Na	*bdl*	*bdl*	bdl	0.16 (13)
K	0.01 (0)	0.01 (0)	0.03 (1)	0.02 (0)
F	0.87 (1)	0.88 (4)	0.52 (15)	1.01 (10)
OH	2.13 (1)	2.12 (4)	7.48 (15)	6.99 (10)
H_2O	4.97 (19)	5.11 (34)	7.98 (291)	6.14 (20)
Σcat.	4.99 (2)	5.01 (2)	10.81 (23)	11.13 (22)
F/(F+OH)	0.29 (0)	0.29 (1)	0.06 (2)	0.13 (1)

Wavellite calculated on 19 electrical charges - Hydroxyls calculated by difference on hydroxyl site (3-F)
Turquoise calculated on 40 electrical charges - Hydroxyls calculated by difference on hydroxyl site (8-F)
H2O calculated by difference on total measured and calculated hydroxyls groups

4.6. Transition metal phosphates

Turquoise – $CuAl_6(PO_4)_4(OH)_8 \bullet 4H_2O$

Turquoise is a very common mineral in Montebras, giving bluish to greenish tint to altered mass of phosphates (Fig. 9b). Textures vary from massive crusts to vesicular assemblage with

wavellite, variscite and kaolinite. Microprobe analyses in massive turquoise veins give the following composition $Cu_{0.88}Fe_{0.02}Ca_{0.02}Al_{5.97}(PO_4)_{4.03}(OH_{7.24}F_{0.41})\bullet 4.00H_2O$ with no visible cathodoluminescence (Table 7).

Triplite – *Mn_2PO_4F*

Triplite is an uncommon microscopic phase with a chemical composition $(Mn_{1.90}Fe_{0.04}Ca_{0.03})(PO_4)_{1.02}(F_{1.00}OH_{0.02})$ (Table 8).

Eosphorite – *$MnAlPO_4(OH)_2\bullet H_2O$*

Eosphorite occurs as yellowish inclusions in amblygonite and as a filling in some quartz veins where it forms subhedral crystals up to 1mm in length. Average chemical analysis is $(Mn_{0.68}Fe_{0.28}Ca_{0.01})Al_{0.98}(PO_4)_{1.02}(OH_{1.96}F_{0.04})_{2.00}\bullet 1.06H_2O$ (Table 8), similar to the ernstite variety (Von Seegiler and Mucke, 1970). The $Mn^{2+} \Leftrightarrow (Fe,Ca)^{2+}$ substitution varies from 0.76 to 0.64 Mn.p.f.u.

Table 8. Composition of eosphorite and triplite

Sample	MONT5	MONT5	MONT5	MONT2
phase	Eosphorite	Eosphorite	Eosphorite	Triplite
n	8	3	3	4
P_2O_5	31.41 (52)	31.31 (52)	31.81 (11)	32.23 (64)
SiO_2	0.04 (2)	0.05 (2)	0.04 (1)	*bdl*
Al_2O_3	21.57 (33)	21.41 (31)	21.95 (23)	0.04 (1)
FeO	8.54 (75)	9.88 (113)	8.01 (122)	1.96 (8)
MnO	20.86 (67)	20.49 (150)	21.83 (90)	59.99 (53)
CuO	*bdl*	*bdl*	0.10 (4)	*n.a.*
MgO	*bdl*	*bdl*	*bdl*	*bdl*
CaO	0.40 (9)	0.20 (4)	0.06 (1)	0.71 (1)
SrO	*bdl*	*bdl*	*bdl*	0.10 (2)
BaO	*bdl*	*bdl*	*bdl*	*bdl*
Na_2O	*bdl*	*bdl*	0.08 (1)	*bdl*
F	0.54 (32)	0.13 (23)	0.12 (14)	*8.50* (45)
H2O	16.07 (75)	15.88 (98)	15.31 (17)	*bdl*
Total	99.64 (34)	99.58 (29)	99.44 (11)	103.62 (102)
Total O =F	99.41 (26)	99.53 (22)	99.38 (14)	100.04 (100)
P	1.02 (1)	1.02 (1)	1.02 (1)	1.02 (1)
Si	*bdl*	*bdl*	*bdl*	*bdl*
Al	0.98 (2)	0.97 (2)	0.98 (1)	*bdl*
Fe	0.27 (3)	0.32 (4)	0.25 (4)	0.04 (0)
Mn	0.68 (2)	0.67 (4)	0.70 (3)	1.90 (2)
Cu	*bdl*	*bdl*	*bdl*	*n.a.*
Mg	*bdl*	*bdl*	*bdl*	*bdl*
Ca	0.02 (0)	0.01 (0)	*bdl*	0.03 (0)
Sr	*bdl*	*bdl*	*bdl*	*bdl*
Ba	*bdl*	*bdl*	*bdl*	*bdl*
Na	*bdl*	*bdl*	0.01 (0)	*bdl*
F	0.07 (4)	0.02 (3)	0.01 (2)	*1.00* (5)
OH	1.93 (4)	1.98 (3)	1.99 (2)	0.02 (2)
H2O	1.10 (11)	1.05 (16)	0.95 (4)	
Σcat.	2.99 (1)	3.00 (0)	2.98 (0)	2.99 (0)
F/(F+OH)	0.03 (2)	0.01 (1)	0.01 (1)	0.98 (0)

Eosphorite calculated on 10 electrical charges - Hydroxyls calculated by difference on hydroxyl site (2-F)
Triplite calculated on 9 electrical charges - Hydroxyls calculated by difference on fluorine site (1-F)
H2O calculated by difference on total measured and calculated hydroxyls groups

4.7. Other phosphates

Phase F – *Na-Al-P-F*

In lacroixite-fluorapatite veins cross-cutting viitaniemiite-bearing amblygonite, phase F is observed as large colourless patches of 100 x 400 μm (Fig. 1a$_1$). No pleochroism is observed and birefringence is extremely low (~0.001) (Fig. 1a$_2$). In cathodoluminescence, phase F shows a bright

vermilion colour (Fig. 1a$_3$, 10). Microprobe analyses (WDS and EDS) show a very high content in fluorine (up to 56 wt.% F) and a poorly defined formula of $Na_{0.99}(Al_{0.77}P_{0.23})(F_{3.44}OH_{0.55})$ based on 4 anions (Table 9).

Hypotheses on the nature of this solid phase are the synthetic compound $NaAlF_4$, which shares a low birefringence and very low refractive index (Liu et al., 2011) but is known to be metastable at room temperature and decomposes into chiolite and AlF_3 or melts at higher temperatures (>500ºC) (Bjorseth et al., 1986, Zaitseva et al., 2009). The significant presence of phosphorus (~13 wt.% P_2O_5) and the very low birefringence (possibly isotropic) suggest that this phase could be a Na-Al fluoride xerogel where it is known that phosphorus (as PO_4 groups) has a complete solubility (Thisted et al., 2006, Kucharik and Vasilijev, 2008). Regardless of the exact nature of this phase, the association of sodium aluminofluoride with phosphates could be an analogue petrological setting to the association cryolite-viitaniemiite in Francon Quarry, Quebec (Tarassof et al., 2006, Ramik et al., 1983).

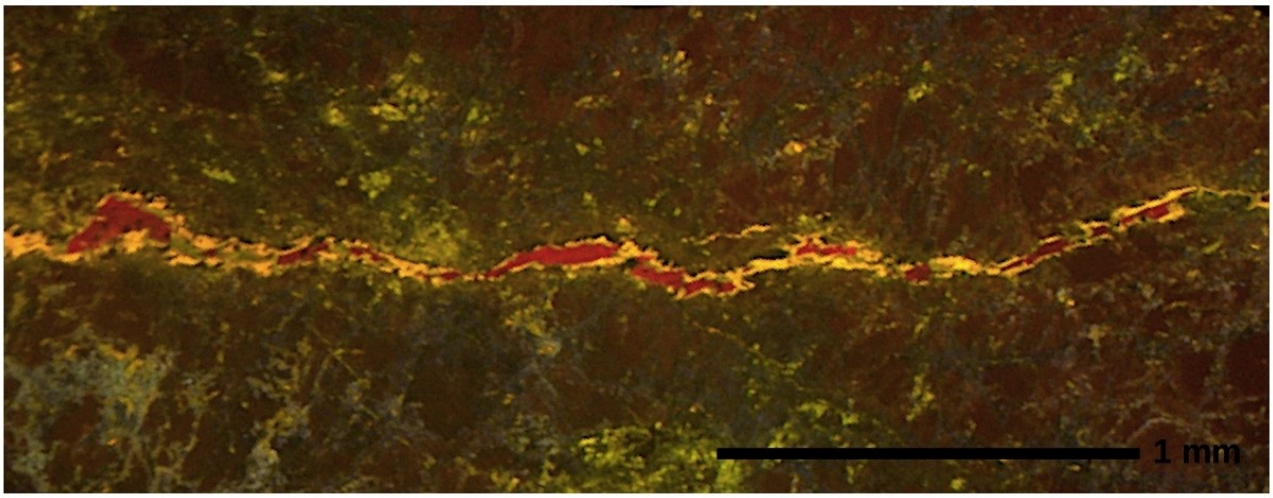

Figure 10. Vein of Phase F (crimson red) filled with two phases of lacroixite (yellow and blue) in an altered primary and secondary amblygonite (brown red) containing diffuse lacroixite (yellow and blue) and some apatite patches (bright yellow) in CL-PPL (Sample MONT 2).

Table 9. Composition of phase F

Sample *phase* n	MONT2 7	MONT2 6	MONT2 F-correction 8
P_2O_5	13.30 (72)	12.86 (36)	12.23 (87)
Al_2O_3	27.49 (45)	27.29 (19)	37.15 (115)
FeO	0.05 (3)	*bdl*	*n.a.* (0)
MgO	0.02 (1)	*bdl*	*n.a.* (0)
MnO	0.13 (2)	0.13 (6)	0.08 (4)
CuO	*bdl*	*bdl*	*n.a.* (0)
CaO	0.16 (3)	0.27 (26)	0.19 (4)
Na_2O	*25.29* (33)	24.58 (29)	23.49 (134)
F	56.35 (87)	53.94 (82)	46.98 (76)
H_2O	2.21 (62)	3.93 (33)	11.01 (233)
Total	125.12 (96)	123.07 (19)	120.13 (199)
Total O =F	101.40 (78)	100.36 (29)	100.35 (179)
P	0.23 (1)	0.22 (1)	0.22 (1)
Al	0.67 (2)	0.65 (1)	0.95 (5)
Fe	*bdl*	*bdl*	*n.a.* (0)
Mg	*bdl*	*bdl*	*n.a.* (0)
Mn	*bdl*	*bdl*	*bdl*
Cu	*bdl*	*bdl*	*n.a.* (0)
Ca	*bdl*	*bdl*	*bdl*
Na	1.02 (2)	0.97 (1)	0.98 (7)
F	3.69 (8)	3.47 (5)	3.21 (11)
OH	0.31 (8)	0.53 (5)	0.79 (11)
Σcat.	1.93 (4)	1.85 (1)	2.16 (11)
F/(F+OH)	0.92 (2)	0.87 (1)	0.80 (3)

Mineral F calculated on 4 anions (F+OH) optimised for an average of 2 cations
Hydroxyls calculated by difference on fluorine site for (4-F)

4.8. Non-phosphate phases

Quartz is very common as a late phase forming veins and filling cavities between phosphate crystals (Fig. 9a). However, in the quartzglöcke, its abundance indicates a precipitation at an earlier stage. Feldspars (microcline and albite) are absent from most phosphate pods. Muscovite is a common phase in all phosphates pods as lamellae from 0.1 to 10 mm in amblygonite and often rimmed by fluorapatite. Chemical composition suggests that at best, lithium content is 0.12 a.p.f.u. (Table 10) of the trioctahedral site, compatible with infrared spectra. No lepidolite group micas have

been observed in Montebras in the scope of this study but polylithionite and zinnwaldite are described in other part of the deposit (Marcoux et al., 2021).

Kaolinite is very frequent in altered phosphate pods of Montebras and sometimes occur as a diffuse cement between masses of amblygonite-montebrasite. Its dark blue cathodoluminescence makes it recognisable from turquoise and variscite which show no luminescence. Chemical composition is ideal although infrared spectroscopy show contamination by residual particles of micas that are not visible in optical microscopy (Table 10).

Table 10. Composition of silicates

Sample	MONT2	MONT12	MONT15	MONT15	MONT12	MONT12
phase	Muscovite	Muscovite	Muscovite	Muscovite	Muscovite	Kaolinite
n	3	2	2	2	3	1
P_2O_5	0.04 (2)	bdl	tr.	tr.	bdl	bdl
SiO_2	46.51 (91)	45.98 (85)	45.68 (74)	45.40 (60)	45.88 (35)	42.81
Al_2O_3	36.73 (27)	36.14 (20)	36.14 (16)	35.82 (104)	36.08 (23)	37.84
FeO	bdl	0.52 (1)	0.63 (14)	0.71 (57)	0.72 (2)	0.08
MnO	0.07 (6)	tr.	0.26 (10)	0.18 (3)	0.11 (1)	0.10
CuO	0.07 (3)	tr.	0.09 (13)	tr.	tr.	0.07
MgO	0.03 (2)	0.16 (4)	0.06 (0)	0.06 (3)	0.13 (1)	tr.
CaO	0.06 (4)	tr.	bdl	tr.	0.04 (3)	0.05
SrO	bdl	tr.	0.03 (4)	bdl	bdl	bdl
BaO	bdl	0.08 (6)	bdl	bdl	0.07 (6)	0.15
Na_2O	0.15 (2)	0.33 (7)	0.26 (13)	0.38 (13)	0.34 (3)	tr.
K_2O	10.95 (13)	10.64 (32)	10.73 (4)	10.61 (42)	11.05 (6)	bdl
F	0.86 (2)	1.43 (26)	1.31 (8)	1.31 (6)	1.39 (5)	0.17
H_2O	4.09 (6)	3.78 (7)	3.83 (7)	3.80 (2)	3.81 (2)	13.06
Total	99.62 (107)	99.43 (141)	99.09 (71)	98.72 (14)	99.72 (50)	94.37
Total O =F	99.26 (107)	98.83 (130)	98.54 (75)	98.17 (16)	99.14 (48)	94.31
P	bdl	bdl	bdl	bdl	bdl	bdl
Si	3.10 (2)	3.09 (2)	3.08 (3)	3.08 (4)	3.08 (0)	1.96
Al	2.88 (2)	2.86 (2)	2.87 (4)	2.86 (9)	2.86 (0)	2.05
Fe	bdl	0.03 (0)	0.04 (1)	0.04 (3)	0.04 (0)	bdl
Mn	bdl	bdl	bdl	0.01 (0)	0.01 (0)	bdl
Cu	bdl	bdl	bdl	bdl	bdl	bdl
Mg	bdl	0.02 (0)	0.01 (0)	0.01 (0)	0.01 (0)	bdl
Ca	bdl	bdl	bdl	bdl	bdl	bdl
Sr	bdl	bdl	bdl	bdl	bdl	bdl
Ba	bdl	bdl	bdl	bdl	bdl	bdl
Na	0.02 (0)	0.04 (1)	0.03 (2)	0.05 (2)	0.04 (0)	bdl
K	0.93 (2)	0.91 (4)	0.92 (0)	0.92 (3)	0.95 (1)	bdl
F	0.18 (1)	0.30 (5)	0.28 (2)	0.28 (1)	0.29 (1)	0.02
OH	1.82 (1)	1.70 (5)	1.72 (2)	1.72 (1)	1.71 (1)	4.00
H_2O						
Σcat.	6.95 (2)	6.98 (0)	6.98 (2)	6.99 (3)	7.00 (1)	4.03
F/(F+OH)	0.09 (0)	0.15 (3)	0.14 (1)	0.14 (1)	0.15 (0)	0.01

Micas calculated on 22 electrical charges - Hydroxyls calculated by difference on hydroxyl site (2-F)
Kaolinite calculated on 14 electrical charges - Hydroxyls calculated by difference on hydroxyl site (4-F

Cassiterite is a common phase observed in all samples. Grains are yellowish to brown, subhedral and disseminated in phosphates pods. In quartz veins, small trails of kidney-shaped grains with colours ranging from yellow to orange-brown, sometimes almost opaque occurs (Fig. 11b). These grains show an important zonation and a complex convoluted internal texture. Darker grains with similar features are also found as rims around stannoidite (Fig. 11a). The chemical composition of these grains appears to be Fe-rich (up to 35% substitution of Sn) cassiterite with minor concentrations of Cu, Nb and Ta. These chemical properties, the gel-like textures (Fig. 11c) and X-ray diffraction pattern not entirely consistent with cassiterite suggest that this mineral phase is varlamoffite.

Hubnerite and manganotantalite with ixiolite in small dark lamellae have also been observed in altered zones (Fig. 11d).

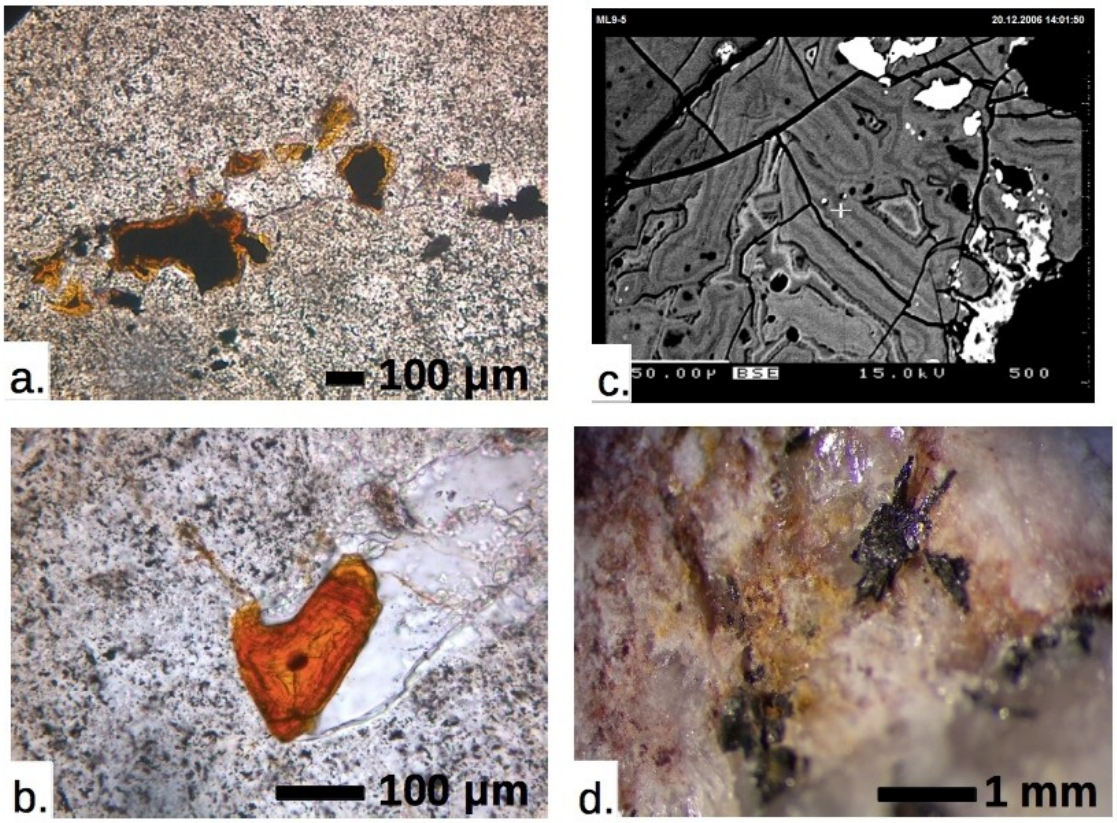

Figure 11. a. Aggregates of stannoidite (black) with varlamoffite rim (brown) in a quartz vein through amblygonite in PPL (Sample MONT 9). b. Varlamoffite grain with quartz in amblygonite (Sample MONT 9). c. Varlamoffite internal zoned textures with stannoidite (bright white), apatite (white) and amblygonite (black) in BSE (Sample MONT 9). d. Macroscopic view of a wolframite grain in altered amblygonite with quartz – yellow zones are possibly tungstite (Sample MONT 8).

Finally, considering the subject of this paper, the following minerals are mentioned in the scientific literature related to phosphate-bearing lithological facies of Montebras. Dufrenite is described as micro-inclusions in variscite while libethenite occurs on feldspars crystals (Lacroix, 1910). Torbernite (as well as cuprite) are associated with tin-rich masses (Lacroix 1901, 1910) and late veins of barite, apatite, fluorite and autunite are common (Aubert, 1969; Marcoux et al., 2021).

The phosphate-rich masses in the quartzglöcke are described as occasionally containing lepidolite (Lacroix, 1895) while the stockscheider pegmatite contains polylithionite-zinnwaldite (Marcoux et al., 2021). This pegmatitic facies is also rich in Sn-W-Nb-Ta mineralisation expressed as wolframite, scheelite, qitianglingite, mawsonite, stannite, tennantite, lollingite, arsenopyrite, chalcopyrite, galena, vinciennite, covellite, bornite and alteration products malachite, chrysocolla and scorodite not encountered in this study (Lacroix, 1901; Aubert, 1969; Marcoux et al., 2021).

5. Discussion

The complexity of these amblygonite-montebrasite assemblages is mostly the result of the post-magmatic alteration process. Although some minor mineral phases (topaz, Fe-Mn phosphates) could be of magmatic origin and associated with the formation of primary amblygonite, it appears that Na-bearing and most alkaline earth (Ca, Sr, Ba) minerals are the result of metasomatic and hydrothermal replacements and precipitation while metal-free alumina-phosphates are linked to relatively low-temperature alteration processes.

5.1. Petrogenesis

The petrogenesis of phosphate pods of the Montebras pegmatite is more extensively developed in Pirard (2022). The pegmatitic cupola is essentially the result of residual melts from the crystallizing microgranite leading to a magma heavily enriched in alkaline elements (Na_2O, K_2O and Li_2O) and high contents in fluorine and phosphorus. Extreme fractionation of this fluorine-rich magma allows the formation of the albite leucogranite and residual melt enrichment in F, P, B, Sn, Nb and Ta, further concentrated by the crystallisation of quartz and alkali feldspars. Magmatic properties allow a possible melt-melt immiscibility and the formation of a phosphorus-rich liquid in the fluorinated phase that would be characterised by a considerably low solidus. Amblygonite and triplite are the primary phases crystallising from such liquid, the former favoured against lithium aluminophosphates due to the separation from the silicate-rich melt at a local scale (London and Burt, 1982; London et al., 1999).

Crystallisation of the magma leads to a separation between what is left of the residual melt and fluids with fluorine remaining in the fluid, quickly followed by the formation of secondary fluorine-rich phases (replacement amblygonite, lacroixite), as the system cooled down by the precipitation of quartz, micas, eosphorite and apatite in veins. As fluorine content in fluids have dropped considerably, F-poor ternary montebrasite crystallises in those veins. However, these fluorine levels are still high enough for further precipitation of lacroixite, viitaniemiite and mineral D and eventually phase F.

Further cooling increase calcium activity which becomes more heavily involved in metasomatic reactions. Fluorapatite, mostly absent in the primary (magmatic) assemblage, become very frequent and precipitate in open cavities and replacing earlier phosphates. Na-Ca phosphates (morinite, wardite) would also appear at this stage but further hydrothermal alteration often decomposes these phases in apatite and crandallite group minerals. The seemingly frequent alteration of morinite and wardite into Na-rich apatite could partly explain the rarity of these

minerals in many deposits where fluorapatite, crandallite and hydrated aluminium phosphates abound.

Finally, for low temperature hydrothermalism, magmatic silicates alters into kaolinite and more crandallite group minerals are precipitated. The alteration of copper-bearing sulfide is also triggering the precipitation of turquoise. This phase can be undistinguishable from meteoric alteration although variscite and wavellite are probably form essentially from indirect weathering.

6. References

Aubert, G., 1969. Les coupoles granitiques de Montebras et d'Echassières (Massif Central français) et la genèse de leur minéralisation étain-lithium-tungstène-béryllium. *Mémoire du BRGM*, **46**, 354p.

Balagny, C., 1939. Le mystère de la callaïs. *Fontenay-le-Compte Imp.*, 48p

Baldwin, J.R., Hill, P.G., von Knorring, O. & Oliver, G.J.H., 2000. Exotic aluminium phosphates, natromontebrasite, brazilianite, goyazite, gorceixite and crandallite from rare-element pegmatites in Namibia. *Mineralogical Magazine*, **64(6)**, p1147-1164.

Bjorseth, O., Herstad, O. & Holm J. L., 1986. On the physical and thermodynamic stability of solid sodium tetrafluoroaluminate. *Acta Chemica Scandinavia*, **A40**, p566-571

Burnham, C.W., 1991. LCLSQ version 8.4., least-squares refinement of crystallographic lattice parameters. *Department of Earth and Planetary Sciences*. Harvard University.

Čech, F. & Povondra, P., 1985. Identity of ježekite with morinite. Bulletin de Minéralogie, **108**, p533-539.

Černá, I., Černý, P. & Ferguson, R.B., 1973. The fluorine content and somy physical properties of the amblygonite-montebrasite minerals. *American Mineralogist*, **58**, p291-301.

Charoy, B. & Noronha, F., 1999. Rare-element (Li-rich) granitic and pegmatitic plutons: a primary or superimposed signature. *Revista Brasileira de Geociencias*, **29(1)**, p3-8.

Daubrée, A., 1868. Apercu historique sur l'exploitation des métaux dans la Gaule. *Revue Archéologique*, **17**, p298-313.

De Cessac, M.P. & Chaussat, M.P., 1886. Montebras, son tumulus, ses mines d'étain. *Bulletin de la Société des Sciences Naturelles et Archéologiques de la Creuse*, 18p.

Dias, I.N., Pinheiro, M.V.B., Moreira, R.L., Krambrock, K., Guedes, K.J., Menezes Filho, L.A.D., Karfunkel, J., Schnellrath, J. & Scholz, R., 2011. Spectroscopic characterization of transition metal impurities in natural montebrasite/amblygonite. *American Mineralogist*, **96**, p42-52.

Dudoignon, P., Beaufort, D. & Meunier, A., 1988. Hydrothermal and supergene alterations in the granitic cupola of Montebras, Creuse, France. *Clays and Clay Minerals*, **36(6)**, p505-520.

Eggins et al., 1998

Fransolet, A.-M. & Tarte, P., 1977. Infrared spectra of analyzed samples of the amblygonite-montebrasite series: a new rapid semi-quantitative determination of fluorine. *American Mineralogist*, **62**. p559-564.

Fransolet, A.-M., Fontan, F. & de Parseval, P., 2007. Natromontebrasite, a discredited mineral species. *Canadian Mineralogist*, **45(2)**, p391-396

Griffin, W.L., Powell, W., Pearson, N.J. & O'Reilly, S.Y., 2008. GLITTER: data reduction software for laser ablation ICP-MS. http://www.*glitter*-gemoc.com

Kallio, P., 1978. A new X-ray method for the estimation of fluorine content in montebrasites. *American Mineralogist*, **63**, p1249-1251.

Kucharik, M., & Vasiljev, R., 2008. Solubility of $AlPO_4$ and $NaVO_3$ in NaF-AlF_3 melts. *Journal of Chemical and Engineering Data*, **53**, p1817-1819.

Lacroix, A., 1891. Note préliminaire sur un minéral nouveau de Montebras (Creuse). *Bulletin de la Société française de Minéralogie*, **14**, p187-189.

Lacroix, A., 1895. Minéralogie de France et de ses colonies, T.1., *Béranger*, Paris, 721p.

Lacroix, A., 1901. Minéralogie de France et de ses colonies, T.3., *Béranger*, Paris, 818p.

Lacroix, A., 1910. Minéralogie de France et de ses colonies, T.4., *Béranger*, Paris, 923p.

Lahti, S.I., 1981. On the granitic pegmatites of Eräjärvi area in Orivesi, Southern Finland. *Geological Survey of Finland*, **314**, 82p.

Liferovich, R.P., Yakovenchuk, V.N., Pakhomovsky, Y.A., Bogdanova, A.N, & Stümpel, G., 1999. Crandallite, goyazite and gorceixite from the Kovdor massif, Russia. *Neues Jahrbüch für Mineralogie, Monatshefte*, **4**, p145-166.

Liu. Q.-J., Liu, Z-.T., Feng, L.-P & Tian, H., 2011. First-principles study of structural, elastic, electronic and optical properties of orthorhombic $NaAlF_4$. *Computational Materials Science*, **50**, p2822-2827.

London, D. & Burt, D.M., 1982. Chemical models for lithium aluminosilicates stabilities in pegmatites and granites. *American Mineralogist*, **67**, p494-509.

London, D., Wolf, M.B., Morgan VI, G.B. & Gallego Garrido, M., 1999. Experimental silicate-phosphate equilibria in peraluminous granitic magmas with a case study of the Albuquerque batholith at Tres Arroyos, Badajoz, Spain. *Journal of Petrology*, **40**, p215-240.

Mallard, E., 1859. Géologie de la Creuse. Journal de voyage d'E Mallard (1857-1860). *Mémoire de la Société des Sciences Naturelles et Archéologiques*. Creuse, **22**, 141p.

Marcoux, E., Barré, B., Pichavant, M. & Poujol, M., 2021. Age et genese de la coupole granitique a métaux rares (sn, Li, Nb-Ta, W) de Montebras (Creuse, Massif central français). *Earth Sciences Bulletin*, **192(16)**, 33p.

Mason, B., 1941. Minerals of the Varutrask pegmatite. XXIII. Some iron-manganese phosphate minerals and their alteration products, woth special reference to material from Varutriisk. **63**, p117-165.

Melleton, J., Gloaguen, E. & Frei, D., 2015. Rare-elements (Li-Be-Ta-Sn-Nb) magmatism in the European Variscan Belt, a Review. *13th SGA Biennial Meeting 2015, Proceedings*, **2**., p807-810.

Milton, C., Axelrod, J.M., Carron, M.K. & Stearns MacNeil, F., 1958. Gorceixte from Dale County, Alabama, *American Mineralogist*, **43**, p688-694.

Moissenet, M.L., 1871. Mémoire sur une nouvelle espèce minérale rencontrée dans le gîte d'étain de Montebras (Creuse). Annales des Mines, **20(4)**, p1-21.

Moore, P.B., 1982. Pegmatite minerals of P(V) and B(III). *In:* P. Černý. Ed., Granitic pegmatites in Science and Industry. *Mineralogical Association of Canada, Short Course Handbook*, **8**, p267-291.

Moss, A.A., Fejer, E.E. & Embrey, P.G., 1969. On the X-ray identification of amblygonite and montebrasite. *Mineralogical Magazine*, **37(287)**, p414-422.

Nagaraja, R., Pushpa Manjari, V., Sailaja, B. & Ravikumar, R.V.S.S.N., 2017. A novel orange emitting Sm^{3+} ions doped $NaCaAlPO_4F_3$ phosphor: Optical and luminescence properties. *Journal of Molecular Structure*, **1130**, p96-102.

Nicolas, J., & Rosen, A., 1966. Phosphates hydrothermaux de basse température et kaolinisation: la gorceixite du massif des Colettes (Allier) et les minéraux associés (hinsdalite). *Bulletin de la Société française de Minéralogie et de Cristallographie*, **86**, p379-385.

Petrík, I., Kubis, M., Konecny, P., Broska, I. & Malachovsky, P., 2011. Rare phosphates from the Surovec Topaz – Li-Mica Microgranite, Gemeric Unit, Western Carpathians, Slovak Republic: Role of F/H_2O of the melt. *The Canadian Mineralogist*, **49**, p521-540.

Pirard, C. 2022. Comparative study of alteration sequences in pegmatitic aluminium phosphates.

Pushpa Manjari, V., Rama Krishna, Ch., Venkata Reddy, Ch. & Ravikumar, R.V.S.S.N., 2014. Synthesis and spectral investigations of Cu(II) ion-doped $NaCaAlPO_4F_3$ phosphor. *Luminescence*, **29**, p1123-1129.

Ramik, R.A., Sturman, B.D., Roberts, A.C. & Dunn, P.J., 1983. Viitaniemiite from the Francon Quarry, Montreal, Quebec. *Canadian Mineralogist*, **21**, p499-502.

Shirose, Y. & Uehara, S., 2014. Secondary phosphates in montebrasite and amblygonite from Nagatare, Fukuoka Prefecture, Japan. *Journal of Mineralogical and Petrological Sciences*, **109**, p103-108.

Spandler, C., Pettke, T. & Rubatto, D., 2011. Internal and external fluid sources for eclogite-facies veins in the Monviso meta-ophiolite, Western Alps: Implications for fluid flow in subduction zones. *Journal of Petrology*, **52(6)**, p1207-1236.

Stevko, M., Uher, P., Sejkora, J., Malikova, R., Skoda, R. & Vaculovic, T., 2015. Phosphate minerals from the hydrothermal quartz veins in specialized S-type granites, Gemerska Poloma (Western Carpathians, Slovakia). *Journal of Geosciences*, **60**, p237-249.

Tarassoff, P., Horváth, L., & Pfenninger-Horváth, E., 2006. The Francon Quarry, Montréal, Québec. *The Mineralogical Record*, **37**.

Taylor, M., Smith, R.W. & Ahler, B.A., 1984. Gorceixite in topaz greisen assemblages, Silvermine area, Missouri. *American Mineralogist*, **69**, p984-986.

Thisted, E.W., Haarberg, G.M. & Thonstad, J., 2006. Solubility of $AlPO_4$ in cryolite melts. *Thermochimica Acta*, **447**, p41-44.

Von Seeliger, E. & Mücke, A., 1970. Ernstit, ein neues Mn^{2+}-Fe^{2+}-Al phosphat un seine beziehungen zum Eosphorit. *Neues Jahrbüch fur Mineralogie, Monatschefte*, p289-298.

White, J.S., 1981. Barian goyazite from Brazil., *The Mineralogical Record*, p379.

Zaitseva, J.N., Yakimov, I.S. & Kirik, S.D., 2009. Thermal transformation of quaternary compounds in NaF-CaF_2-AlF_3 system. *Journal of Solid State Chemistry*, **182**, p2246-2251.